

DISS. ETH NO. XX

Eco-evolutionary processes in ecological and economic systems

Confronting dynamical models and data

A thesis submitted to attain the degree of
DOCTOR OF SCIENCES of ETH ZURICH
(Dr. sc. ETH Zurich)

presented by

VICTOR BOUSSANGE

M.Sc. Energy and environmental sciences, Institut National des Sciences
Appliquées de Lyon
born January 10th, 1995
citizen of Bordeaux, France

accepted on the recommendation of

Prof. Dr. Loïc Pellissier, (doctoral thesis supervisor), examiner
Prof. Dr. Didier Sornette, co-examiner
Prof. Dr. Arnulf Jentzen, co-examiner
Prof. Dr. Samir Suweis, co-examiner

2022



Forward and inverse modelling of eco-evolutionary
dynamics in biological and economic systems

Victor Boussange
August 29, 2022

Version: 0.0.1

Victor Boussange

Forward and inverse modelling of eco-evolutionary dynamics in biological and economic systems

August 29, 2022

Reviewers: Didier Sornette Samir Suweis and Arnulf Jentzen

Supervisors: Loïc Pellissier

ETH Zürich

Ecology Landscape and Evolution

Institute of Terrestrial Ecosystems

Department of Environmental Sciences

Universitätstrasse 18

8055 and Zürich

Summary

Ecological and economic systems are complex adaptive systems (CAS): they are systems that are composed of many entities with heterogeneous characteristics, which interact and experience selection processes. Those processes act at the entity level, but are key in determining the macroscopic behaviour at the system level, a feature that make those systems unique. For instance, the diversity of species within an ecosystem results from a hierarchy of processes acting at different scales of time and space, comprising the variations experienced by single organisms, their interactions, and selection pressure acting upon populations. Analogously, economic growth at the level of a country is greatly affected by its ensemble of economic actors, their interactions, and the selection pressure they experience. Despite the complexity of the processes driving their dynamics, regularities at the macroscopic level emerge in ecological and economic systems. This is the case of large-scale spatial patterns of biodiversity and differences in economic growth across countries, calling for a mechanistic understanding of the essential mechanisms that generate them.

Recently, a considerable interest has grown up around the interplay between ecological processes, the processes that regulate interactions between organisms, and evolutionary processes, the change of the characteristics of biological populations over time, to explain current biodiversity patterns. Analogous economic processes have been proposed to explain differences in economic growth across nations. Nonetheless, a quantitative investigation of their importance is missing. Determining how those patterns can emerge from eco-evolutionary processes is required to improve our current understanding. This project delivers new quantitative insights following a unique approach that combines dynamical eco-evolutionary models and empirical data.

Simulations of eco-evolutionary models and their integration with empirical data pose several methodological challenges that we address in the first part of this project. Entities in CAS have distinct quantitative attributes that determine their fitness in a given environment. Accounting for the variety of these characteristics leads to models with a high dimensionality, associated to a large if not prohibitive computational cost preventing its simulation. In particular, partial differential equation (PDE) models, which can encode eco-evolutionary processes acting upon entities defined

by many characteristics, are cursed by their dimensionality. To this aim, we develop machine learning algorithms that break down the curse of dimensionality. Such algorithms rely on neural networks to approximate the solution to PDE models. An other difficulty consists in confronting eco-evolutionary models outputs to data, since those models cannot be manipulated with standard statistical techniques. We apply methods commonly employed in the training of neural networks, together with model selection techniques, to infer fundamental mechanisms that might have generated the patterns under investigation. Altogether, the methods permit efficient model simulations and their integration with empirical data, allowing to deliver quantitative answers to the motivated research questions.

In the second part, we make use of the above techniques to study eco-evolutionary models and to test them against data, to explore hypotheses on the fundamental mechanisms that drive patterns of biodiversity and economic growth. From one hand, we explore how eco-evolutionary processes, in combination with complex landscape topologies, can explain patterns of species diversity. To this aim, we develop and analyse an eco-evolutionary model on spatial graphs, to understand how the combination of eco-evolutionary processes and spatial structure might have shaped biodiversity patterns that are found in complex landscapes such as mountain regions.

On the other hand, we investigate how eco-evolutionary processes can provide new insights in the understanding of economic dynamics. We proceed by developing a simple eco-evolutionary model which explanatory power we test against long time series that proxy the dynamics of the size of economic sectors.

Overall, this project delivers quantitative insights on how the interplay between ecological and evolutionary processes is shaping the features of the world that surrounds us.

Résumé

- Same as above, but in french

Contents

1	Introduction	1
1.1	Context of modelling	1
1.2	Complex adaptive systems	2
1.3	Eco evolutionary processes	5
1.4	Models and challenges	5
1.5	Machine learning : opportunities	6
1.6	Learning from models	7
1.7	Thesis outline	8
2	Eco-evolutionary model on spatial graphs reveals how habitat structure affects phenotypic differentiation	11
2.1	Introduction	13
2.2	Results	15
2.2.1	Eco-evolutionary model on spatial graphs	15
2.2.2	Deterministic approximation of the population dynamics under no selection	17
2.2.3	Effect of graph topology on neutral differentiation under no selection	18
2.2.4	Deterministic approximation of the population dynamics and adaptation under heterogeneous selection	21
2.2.5	Effect of graph topology on adaptive differentiation under heterogeneous selection	23
2.2.6	Effect of habitat assortativity on neutral differentiation under heterogeneous selection	25
2.3	Discussion	28
2.4	Methods	30
2.4.1	Mean field approximation	30
2.4.2	Adaptive dynamics on graphs	31
2.4.3	Numerical simulations	32
2.4.4	Statistics and reproducibility	33
2.A	Supplementary Note	40
2.A.1	Mathematical construction of the model	40
2.A.2	Deterministic approximation	41

2.A.3	Trait-dependent competition	44
2.A.4	Derivation of the habitat assortativity metric r_Θ in binary environments	44
2.B	Supplementary Figures	47
2.C	Supplementary Tables	58
3	Curriculum vitae	63
4	CV	65

Introduction

1.1 Context of modelling

- human curiosity: build models of what surrounds us
 - Nature has been fascinating since the beginning of humankind.
 - * Human's curiosity lead us to propose models capturing our belief on how things work. Those were mainly conceptual models.
 - The scientific method started with the Enlightenment, during the 18th century (Holmes, 1997).
 - * Isaac Newton became the revered founder of modern Mechanics due to his intuition, gathered by empirical evidence, about a possible mathematical formalization for the law of universal gravitation. [Equations2021]
 - * 20th century: logical empiricism dominated the philosophy of science and scientists searched for fundamental theoretical principles explaining the laws of nature, with physics at the central stage (Okasha 2002)
 - * in biology, natural history mainly (classification of living organisms without further questioning).
 - why is it that we better understand the motion of planets, or the surface of the moon, than e.g. the mechanisms that drive our fingers? (REF)
 - biological world poses obstacles in finding laws: nonlinear processes and complexity of processes and spatial and time scales
 - The mathematicalisation of soft science was driven by inspiration from physics

* From the 1700s on, nature has been increasingly described by mathematical equations, with differential or difference equations forming the basic framework for describing dynamics. The use of mathematical equations for ecological systems came much later, pioneered by Lotka and Volterra, who showed that population cycles might be described in terms of simple coupled nonlinear differential equations. It took decades for Lotka-Volterra-type models to become established, but the development of appropriate differential equations is now routine in modeling ecological dynamics. There is no question that the injection of mathematical equations, by forcing clarity and precision into conjecture(2), has led to increased understanding of population and community dynamics. As in science in general, in ecology equations are a key method of communication and of framing hypotheses. These equations serve as compact representations of an enormous amount of empirical data and can be analyzed by the powerful methods of mathematics [0].

- AI era
- Scientific revolution of Darwin thinking, by Kuhn's definition (Dawkins 2010)
- Universal Darwinism
- more than a curiosity : a necessity
 - Approaching a state shift in Earth biosphere: [0]
- Bridge those models with data

1.2 Complex adaptive systems

- A central aim in the discipline of Ecology is to determine the underlying causes of variation in the abundance and distribution of species.
- Ecological and economic systems are complex adaptive systems (CAS): they are systems that are composed of many entities with heterogeneous characteristics, which interact and experience selection processes. Those processes act at the individual level, but are key in determining the macroscopic behaviour at the system level, a feature that makes those systems unique.

- Complex interconnected systems pose a major challenge to scientific study in ecology and economics [0] (and references therin).
 - the common approach of reducing these systems to linearly independent components overlooks important interactions for the sake of computational tractability
 - statistical frameworks (e.g., PCA, GLM, multivariate autoregressive models), assume that causal factors do not interact with each other and have independent or additive effects on a response variable,
 - * simplification leads to problems in identifying associations (refs 5-6 of [0])
 - * cannot predict out-of sample behaviour
 - complex equation-based model explicitly accounting for each interaction have great intuitive appeal
 - * but those models suffer from their many parameters to be precisely determined given the available data (curse of dimensionality (ref 9 [0]))
 - * problem is amplified because in biological fields the relevant units may not behave according to the fundamental equations.

Biological systems

- Biodiversity results from a hierarchy of processes acting at different scales of time and space. Variations experienced by organisms, their interactions between them and with the environment, and selection pressure acting upon groups of organisms are of particular relevance for explaining differences in species richness at the ecosystem levels.
 - The synthetic theory of evolution (see e.g. Gayon 2003): with genetics (Mendel) and DNA (James Watson and Francis Crick)
 - *Nothing in biology makes sense except in the light of evolution* (Dobzhansky 1973)
- explanation for the main principles underlying the emergence of biodiversity: multiple processes that interact at different scale in space and time
 - allopatric speciation

- ecological speciation
- dispersal
- adaptation
- those processes interact simultaneously within the surrounding environment
- Traits: measurable characteristics that reflect and shape evolutionary history (Darwin 1859). Natural selection promotes the evolution of traits that optimize species survival under specific environmental conditions..

Economic systems

- The economic trajectory of a country is greatly affected by the ensemble of economic actors and their interactions, that structure its economy. Firms are adaptive entities that respond to the environment in which they operate according to their characteristics, that vary over time. By interacting together and experiencing selection pressure, they determine economic growth at the country level.
- Universal Darwinism

Research questions

- Despite the intrinsic variability of the entities that compose them, and despite the complexity of the processes driving their dynamics, regularities at the macroscopic level emerge in ecological and economic systems. This is the case of large-scale spatial patterns of biodiversity and differences in economic growth across countries, calling for a mechanistic understanding of the essential mechanisms that generate them.
- Multiple arrangements of parts that result in a complex set of effects in a system are defined as mechanisms (Dawkins 2010)

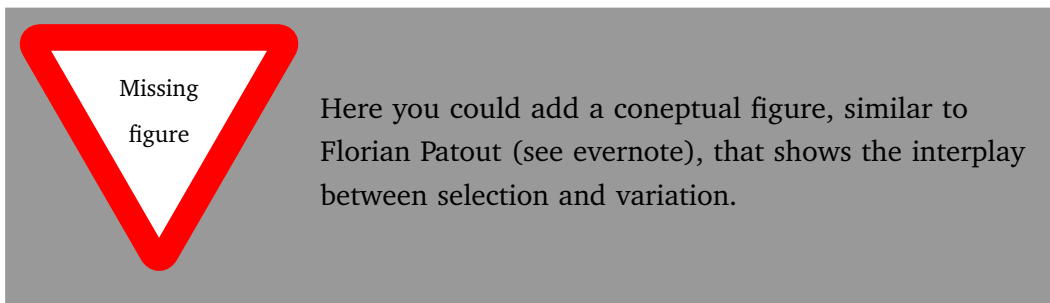
1.3 Eco evolutionary processes

- Eco-evolutionary processes and analogous economic processes acting upon firms have been proposed to play a major role in the emergence of macroscopic patterns in ecological and economic systems. Nonetheless, a quantitative investigation of their importance is missing.
 - The interplay between ecological processes, the processes that regulate interactions between organisms, and evolutionary processes, the change of the characteristics of biological populations over time, has recently received increasing attention to explain current biodiversity patterns.
 - Analogous economic processes have been proposed to explain differences in economic growth across nations.
- A quantitative investigation of how those patterns can emerge from eco-evolutionary processes is required to improve our current understanding and generate a parsimonious theory with predictive power. This defines the goal of this project, which undertakes this investigation through a unique approach that consists in confronting quantitative eco-evolutionary models to empirical data.

1.4 Models and challenges

- Eco-evolutionary models are complicated and necessitate the use of computers to be simulated and analysed against data. This poses a number of methodological challenges that we address in the first part of this project.
 - Entities in CAS have distinct quantitative attributes that determine their fitness in a given environment. Accounting for the variety of these characteristics leads to models with high dimensionality, associated to a high if not prohibitive computational cost preventing its simulation.
 - * The model zoo
 - Agent Based model: hard to scale up
 - PDE: hard to scale up

- In particular, partial differential equation (PDE) models, which can encode eco-evolutionary processes acting upon entities defined by many characteristics, are cursed by their dimensionality.
 - Machine learning: scale up
 - * To this aim, we develop machine learning algorithms that break down the curse of dimensionality by relying on neural networks to approximate the solution to PDE models.
- An other difficulty consists in confronting eco-evolutionary models with data, since those models cannot be manipulated by standard statistical techniques.
 - * We apply methods commonly employed in the training of neural networks, together with model selection techniques, to infer from candidate models fundamental mechanisms that characterise the patterns under investigation.
- The machine learning approximations that we develop allow for efficient model simulations, that we combine with training techniques and model selection methods to explore the motivated research question.



1.5 Machine learning : opportunities

- State of the art machine learning techniques have yielded transformative results across divers scientific disciplines [REF], but rely on a large amount of data [REF], while environmental sciences rely in a small data regime where those techniques are typically not suited [Raissi2019a]. Recently, physics informed machine learning has emerged as a tool to constrain fully parametric methods with scientific knowledge, for data efficiency and extrapolation

[Raissi2019a]. The key idea is to refine the learning with scientific knowledge by adding additional constraints in the objective function, given by ODEs/PDEs models.

- [0]
- [Rolnick2023], Tackling Climate Change with Machine Learning: Changes in climate are increasingly affecting the distribution and composition of ecosystems. This has profound implications for global biodiversity, as well as agriculture, disease, and natural resources such as wood and fish. ML can help by supporting efforts to monitor ecosystems and biodiversity. Monitoring

1.6 Learning from models

- we develop quantitative models that embed general eco-evolutionary processes, and test them against data to explore hypotheses on the fundamental mechanisms that drive patterns of biodiversity and economic growth.
 - From one hand, we explore how eco-evolutionary processes, in combination with complex landscape topologies, can explain patterns of species diversity.
 - To this aim, we develop and analyse an eco-evolutionary model on spatial graphs, to understand how the combination of eco-evolutionary processes and complex landscapes might have shaped biodiversity patterns that are found in complex landscapes such as mountain regions.
 - On the other hand, we investigate how eco-evolutionary processes can provide new insights in the understanding of economic dynamics.
 - We proceed by developing a simple eco-evolutionary model which explanatory power we test against long time series that capture the dynamics of asset size of economic sectors.
- Overall, this project is a step towards providing a useful conceptualisation of fundamental eco-evolutionary mechanisms that shape the features of the world that surrounds us.

1.7 Thesis outline

Part ??

An eco-evolutionary model on spatial graphs

It is not clear how landscape connectivity and habitat heterogeneity influence differentiation in biological populations. To obtain a mechanistic understanding of underlying processes, we construct an individual-based model that accounts for eco-evolutionary and spatial dynamics over graphs. Individuals possess both neutral and adaptive traits, whose co-evolution results in differentiation at the population level. In agreement with empirical studies, we show that characteristic length, heterogeneity in degree and habitat assortativity drive differentiation. By using analytical tools that permit a macroscopic description of the dynamics, we further link differentiation patterns to the mechanisms that generate them. This part provides support for a mechanistic understanding of how landscape features affect diversification.

Part ??

Scientific machine learning for eco-evolutionary modelling

It is a daunting task to obtain an agreement between mechanistic models and real world systems. In particular, there is a need to account for the dimensionality of the evolutionary and spatial structures over which agents interact and evolve. Furthermore, the calibration of such models is difficult. To address the difficulties that arise due to the dimensionality of models, we develop two numerical methods to solve high-dimensional non-local nonlinear PDES that arise in eco-evolutionary models. We implement those methods in a software, HighDimPDE.jl, that integrates within an open source ecosystem for Scientific Machine Learning in the Julia programming language. We further present a scheme to estimate the parameters of a mechanistic model from empirical data sets. We show with analytical arguments that the use of different shallow time series allows for a better estimation than a unique, possibly deeper time series. This part provides ready-to-use modeling tools to address the intrinsic complexity of complex adaptive systems.

Part ??

Bridging eco-evolutionary models and data

Despite evidences that alike biological systems, economic systems are complex adaptive systems that continuously adapt and experience evolutionary processes, economists have discarded biological models and have rather relied on mechanistic models inspired from physics. Building upon an analogy between economic sectors

and biological functional groups, we use a biological model to quantitatively investigate whether eco-evolutionary processes characterise the dynamics of economic sectors. Overall, we find that interactions across economic sectors, evolution of new economic sectors, and international transfers play a major role in the dynamics of economic sectors at the national level. The significance and the strength of such processes strongly vary across countries and correlate with standard macroeconomic indices such as the Economic Complexity Index. We relate such patterns to documented patterns in ecology and evolution. This part provides a new perspective on the understanding of the dynamics of economic systems.

Eco-evolutionary model on spatial graphs reveals how habitat structure affects phenotypic differentiation

by Victor Boussange^{1,2} and Loïc Pellissier^{1,2}

¹ Swiss Federal Research Institute WSL, CH-8903 Birmensdorf, Switzerland

² Landscape Ecology, Institute of Terrestrial Ecosystems, Department of Environmental System Science, ETH Zürich, CH-8092 Zürich, Switzerland

Published in Communications Biology (2022)

doi:10.1038/s42003-022-03595-3

Differentiation mechanisms are influenced by the properties of the landscape over which individuals interact, disperse and evolve. Here, we investigate how habitat connectivity and habitat heterogeneity affect phenotypic differentiation by formulating a stochastic eco-evolutionary model where individuals are structured over a spatial graph. We combine analytical insights into the eco-evolutionary dynamics with numerical simulations to understand how the graph topology and the spatial distribution of habitat types affect differentiation. We show that not only low connectivity but also heterogeneity in connectivity promotes neutral differentiation, due to increased competition in highly connected vertices. Habitat assortativity, a measure of habitat spatial auto-correlation in graphs, additionally drives differentiation under habitat-dependent selection. While assortative graphs systematically amplify adaptive differentiation, they can foster or depress neutral differentiation depending on the migration regime. By formalising the eco-evolutionary and spatial dynamics of biological populations on graphs, our study establishes fundamental links between landscape features and phenotypic differentiation.

2.1 Introduction

Biodiversity results from differentiation processes influenced by the features of the landscape over which populations are distributed [1]. The documentation of high levels of species diversity in mountain regions and riverine systems suggests that complex connectivity patterns and habitat heterogeneity foster differentiation [2, 3, 4, 5]. However, hypotheses formulated based on empirical evidence should be complemented by mechanistic models to crystallise a causal understanding between processes and patterns [6]. While the number of simulation studies is growing steadily [7], such studies often lack a mathematical formalism to facilitate the interpretation of the model outcomes by providing an analytical underpinning to the simulation results [8].

Phenotypic differentiation processes emerge as a result of mutation, selection and migration and can be classified as neutral or adaptive [9]. Neutral differentiation is initiated by the stochastic drift of local phenotypes when spatial isolation and limited dispersal create barriers to gene flow, allowing distinct phenotypes to emerge in spatially structured populations [10]. In contrast, adaptive differentiation results from heterogeneous selection, which promotes distinct, locally well-adapted phenotypes in populations occupying patches with different habitat conditions [11]. The evolution of neutral phenotypes and of adaptive phenotypes are not independent, as selective forces can indirectly select for those neutral phenotypes that happen to be linked to the fittest adaptive phenotypes, a mechanism called the hitchhiking effect [12]. Moreover, selection can generate barriers to gene flow between populations in heterogeneous habitat landscapes [13, 14], a phenomenon coined isolation by environment, which can amplify neutral differentiation. How neutral processes, adaptive processes and their interplay are affected by landscape features is difficult to comprehend without a formalised mechanistic model [15].

Models link patterns to processes [6], and the explicit representation of the landscape within an eco-evolutionary model can lead to a causal understanding of how landscape features shape differentiation. Spatial graphs provide a convenient mathematical representation of landscapes, where vertices represent suitable habitats hosting populations, and edges capture the connectivity between habitats [16]. Under ecological dynamics, metapopulation models have been used to study the role of graph topology in the persistence and stability of metapopulation [17, 18, 19, 20] and community diversity [21, 22, 23]. Evolutionary mechanisms are nevertheless fundamental drivers of diversity, and should therefore be explicitly integrated into models [24]. Evolutionary game theory explores how graph topology impacts the fixation probability and the fixation time of a mutated phenotype [25]. However, the framework does not consider the continuous accumulation of mutations, and is therefore not suited to addressing the emergence of phenotypic differentiation. By combining a metapopulation model with a model of neutral evolution, [26, 27] investigated how graph topology affects neutral diversity. Their approach demonstrated the key role of topological properties in shaping diversity, and its predictions could be matched with empirical data from e.g. river basins [28]. Nonetheless, diversity results from the combination of neutral and adaptive processes developing at the population level. A first principles modelling

approach considering spatial graphs, but also building upon the elementary processes of ecological interactions, reproduction, mutation and migration may therefore be promising to investigate the emergence of diversity.

Stochastic models for structured populations, rooted in the microscopic description of individuals, offer a generic framework for modelling eco-evolutionary dynamics [29, 30]. In particular, these models can capture the interplay between population dynamics, spatial dynamics and phenotypic evolution, while providing a rigorous set-up for analytical investigation. By anchoring this modelling paradigm in a mathematical framework, the work of Champagnat et al. [29] generalises models of population genetics [31] (investigating the evolution of the frequencies of alleles) and quantitative genetics [32, 33, 34] (investigating the evolution of phenotypic traits), which stimulated research into the link between spatial population structure and neutral differentiation. The framework embraces density-dependent selection, which could explain the emergence of phenotypic differentiation from competition processes [11], and how spatial segregation can emerge as a byproduct of these adaptive processes along environmental gradients [35]. Related models have addressed the effects of landscape dynamics and habitat heterogeneity on adaptive differentiation, providing mathematical insights into the dynamics [36, 37, 38, 39, 40, 41]. Because it accounts for finite population size, the baseline model of Champagnat et al. [29] can also capture neutral differentiation dynamics and therefore the coupling between neutral and adaptive processes [42, 43]. Nonetheless, the aforementioned studies were not spatially explicit [42, 43] or they assumed regular spatial structures (regular graphs [36, 37, 38, 41] or continuous space [35, 39, 40]), therefore not addressing the role of the spatial complexity of landscapes. A stochastic individual-based model using spatial graphs as a representation of the landscape could help formalise fundamental links between landscape features and phenotypic differentiation.

A key challenge is to understand how individual dynamics result in the emergence of differentiation in complex landscapes [44]. Here, we investigate how complex connectivity patterns and habitat heterogeneity affect both neutral and adaptive phenotypic differentiation by constructing an individual-based model (IBM) that accounts for eco-evolutionary dynamics on spatial graphs. The individuals disperse between habitat patches and possess co-evolving neutral and adaptive traits. The finite size of local populations generates neutral differentiation by inducing a stochastic drift in the neutral trait evolution, while heterogeneous selection gives rise to adaptive differentiation. Macroscopic properties of the model are analytically tractable, and we obtain a deterministic approximation of population size and adaptive trait dynamics which connects the emerging patterns to the graph properties that generate them. However, neutral differentiation is stochastic by nature, which complicates its analytical underpinning. We therefore rely on numerical simulations of the IBM to measure the effect of graph topology on neutral differentiation. In the case where heterogeneous selection is absent, we investigate how graph topology affects neutral differentiation. In the case of heterogeneous selection, we investigate how the graph topology, in combination with the spatial distribution of habitat types, affects levels of (i) adaptive and (ii) neutral differentiation. By combining analytical methods with numerical simulations, we expect to identify graph properties that determine the level of differentiation. Overall, our study establishes

causal links between landscape properties and population differentiation and contributes to a fundamental understanding of how landscape features promote biodiversity.

2.2 Results

2.2.1 Eco-evolutionary model on spatial graphs

We establish an individual-based model (IBM) where individuals are structured over a trait space and a graph representing a landscape. For the sake of simplicity, we consider the case of asexual reproduction and haploid genetics [29]. Individuals die, reproduce, mutate and migrate in a stochastic fashion, which together results in macroscopic properties. The formulation of the stochastic IBM allows an analytical description of the dynamics at the population level, which links emergent properties to the elementary processes that generate them.

The trait space $\mathcal{X} \subseteq \mathbb{R}^d$ is continuous and can be split into a neutral trait space \mathcal{U} and an adaptive trait space \mathcal{S} . We refer to neutral traits $u \in \mathcal{U}$ as traits that are not under selection, in contrast to adaptive traits $s \in \mathcal{S}$, which experience selection. The graph denoted by G is composed of a set of vertices $\{v_1, v_2, \dots, v_M\}$ that correspond to habitat patches (suitable geographical areas), and a set of edges that constrain the movement of individuals between the habitat patches. We use the original measure of genetic differentiation for quantitative traits Q_{ST} (standing for Q -statistics) in the case of haploid populations [45, 46]. We denote the neutral trait value of the k -th individual on v_i as $u_k^{(i)}$, the number of individuals on v_i as $N^{(i)}$, the mean neutral trait on v_i as $\bar{u}^{(i)}$, and the mean neutral trait in the metapopulation as \bar{u} . It follows that we quantify neutral differentiation $Q_{ST,u}$ as

$$Q_{ST,u} = \sigma_{B,u}^2 / (\sigma_{B,u}^2 + \sigma_{W,u}^2) \quad (2.1)$$

where $\sigma_{B,u}^2 = \mathbb{E} \left[\frac{1}{M} \sum_i (\bar{u}^{(i)} - \bar{u})^2 \right]$ denotes the expected neutral trait variance between the vertices and $\sigma_{W,u}^2 = \frac{1}{M} \sum_i \mathbb{E} \left[\frac{1}{N^{(i)}} \sum_k (u_k^{(i)} - \bar{u}^{(i)})^2 \right]$ denotes the average expected neutral trait variance within vertices. We similarly quantify adaptive differentiation $Q_{ST,s}$.

Following the Gillespie update rule [47], individuals with trait $x_k \in \mathcal{X}$ on vertex v_i are randomly selected to give birth at rate $b^{(i)}(x_k)$ and die at rate $d(N^{(i)}) = N^{(i)}/K$, where K is the local carrying capacity. The definition of d therefore captures competition, which is proportional to the number of individuals on a vertex and does not depend on the individuals' traits (we relax this assumption later on). The offspring resulting from a birth event inherits the parental traits, which can independently be affected by mutations with probability μ . A mutated trait differs from the parental trait by a random change that follows a normal distribution with variance σ_μ^2 (corresponding to the continuum of alleles model [48]). The offspring can further migrate to neighbouring vertices by executing a simple random walk on G with probability m . A schematic overview of the two different settings

considered is provided in Fig. 2.1. Under the setting with no selection, individuals are only characterised by neutral traits so that $\mathcal{X} = \mathcal{U}$. For individuals on a vertex with trait $x_k \equiv u_k$ we define $b^{(i)}(x_k) \equiv b$, so that the birth rate is constant. This ensures that neutral traits do not provide any selective advantage. Under the setting with heterogeneous selection, each vertex of the graph v_i is labelled by a habitat type with environmental condition Θ_i that specifies the optimal adaptive trait value on v_i . It follows that, for individuals with traits $x_k = (u_k, s_k) \in \mathcal{U} \times \mathcal{S}$ on v_i , we define

$$b^{(i)}(x_k) \equiv b^{(i)}(s_k) = b(1 - p(s_k - \Theta_i)^2) \quad (2.2)$$

where p is the selection strength [41]. This ensures that the maximum birth rate on v_i is attained for $s_k = \Theta_i$, which results in a differential advantage that acts as an evolutionary stabilising force. In the following we consider two habitat types denoted by \bullet and \circ with symmetric environmental conditions θ_\bullet and θ_\circ , so that $\Theta_i \in \{\theta_\bullet, \theta_\circ\}$ and $\theta_\circ = -\theta_\bullet = \theta$, where θ can be viewed as the habitat heterogeneity [41].

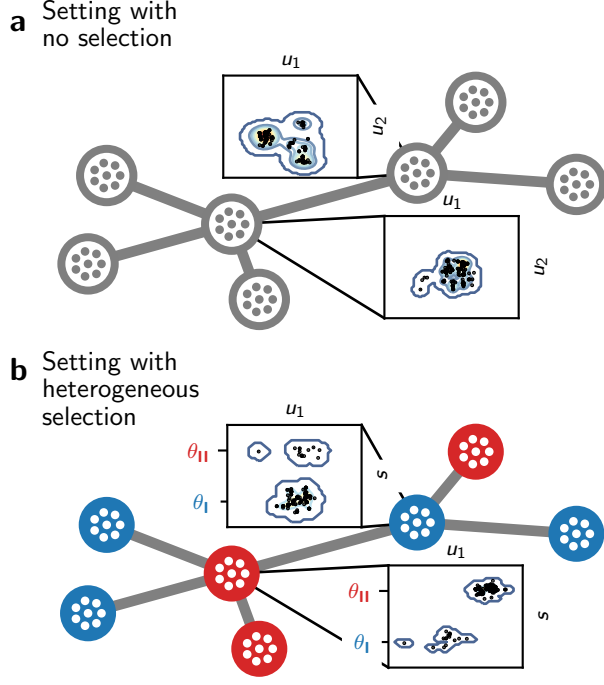


Fig. 2.1: Graphical representation of the structure of individuals in the eco-evolutionary model. (a) Setting with no selection, where individuals are characterised by a set of neutral traits $u \in \mathcal{U}$. The scatter plots represent a projection of the first two components of u for the individuals present on the designated vertices at time $t = 1000$, obtained from one simulation of the IBM. (b) Setting with heterogeneous selection. In this setting, individuals are additionally characterised by adaptive traits $s \in \mathcal{S}$. Blue vertices favour the optimal adaptive trait value θ_{\bullet} , while red vertices favour θ_{\circ} . The scatter plots represent a projection of the first component of u and s for the individuals present on the designated vertices at time $t = 1000$, obtained from one simulation. The majority of individuals are locally well-adapted and have an adaptive trait close to the optimal value, but some maladaptive individuals originating from neighbouring vertices are also present. $m = 0.05$.

2.2.2 Deterministic approximation of the population dynamics under no selection

The model can be formulated as a measure-valued point process ([30] and Supplementary Note). Under this formalism, we demonstrate in the Supplementary Note how the population size and the trait dynamics show a deterministic behaviour when a stabilising force dampens the stochastic fluctuations. This makes it possible to express the dynamics of the macroscopic properties with deterministic differential equations, connecting emergent patterns to the processes that generate them. In particular, in the setting of no selection, competition

stabilises the population size fluctuations, and the dynamics can be considered deterministic and expressed as

$$\partial_t N_t^{(i)} = N_t^{(i)} \left[b(1 - m) - \frac{N_t^{(i)}}{K} \right] + mb \sum_{j \neq i} \frac{a_{i,j}}{d_j} N_t^{(j)} \quad (2.3)$$

where $A = (a_{i,j})_{1 \leq i,j \leq M}$ is the adjacency matrix of the graph G and $D = (d_1, d_2, \dots, d_M)$ is a vector containing the degree of each vertex (number of edges incident to the vertex). The first term on the right-hand side corresponds to logistic growth, which accounts for birth and death events of non-migrating individuals. The second term captures the gains due to migrations, which depend on the graph topology. Assuming that all vertices with the same degree have an equivalent position on the graph, corresponding to a mean field approach (see Methods), one can obtain a closed-form solution from Eq. (2.3) (see Eq. (2.12)), which shows that the average population size \bar{N} scales with $\langle \sqrt{k} \rangle^2 / \langle k \rangle$, where $\langle k \rangle$ is the average vertex degree and $\langle \sqrt{k} \rangle$ is the average square-rooted vertex degree. The quantity $\langle \sqrt{k} \rangle^2 / \langle k \rangle$, denoted as h_d , relates to the homogeneity in vertex degree of the graph and can therefore be viewed as a measure negatively associated with heterogeneity in connectivity. Simulations of the IBM illustrate that h_d can explain differences in population size for complex graph topologies with varying migration regimes (Fig. 2.2a for graphs with $M = 7$ vertices and Fig. S1a for $M = 9$). This analytical result is connected to theoretical work on reaction diffusion processes [49] and highlights that irregular graphs (graphs whose vertices do not have the same degree) result in unbalanced migration fluxes that affect the ecological balance between births and deaths. Highly connected vertices present an oversaturated carrying capacity ($N^{(i)} > bK$, see Methods), increasing local competition and lowering total population size compared with regular graphs (Fig. 2.2a). Because populations with small sizes experience more drift ([31] and Fig. S2), this result indicates that graph topology affects neutral differentiation not only through population isolation, but also by affecting population dynamics.

Nonetheless, the stochasticity of the processes at the individual level can propagate to the population level and substantially affect the macroscopic properties. In particular, neutral differentiation emerges from the stochastic fluctuations of the populations' neutral trait distribution. These fluctuations complicate an analytical underpinning of the dynamics, and in this case simulations of the IBM offer a straightforward approach to evaluate the level of neutral differentiation.

2.2.3 Effect of graph topology on neutral differentiation under no selection

We study a setting with no selection and investigate the effect of the graph topology on neutral differentiation. When migration is limited, individuals' traits are coherent on each vertex but stochastic drift at the population level generates neutral differentiation between the vertices. Migration attenuates neutral differentiation because it has a correlative effect

on local trait distributions. Following [26, 21, 22], we expect that the intensity of the correlative effect depends on the average path length of the graph $\langle l \rangle$, defined as the average shortest path between all pairs of vertices [50]. For a constant number of vertices, $\langle l \rangle$ is strictly related to the mean betweenness centrality and quantifies the graph connectivity [50]. High $\langle l \rangle$ implies low connectivity and a greater isolation of populations, and hence we expect that graphs with high $\langle l \rangle$ are associated with high differentiation levels. We consider various graphs with an identical number of vertices and run simulations of the IBM to obtain the neutral differentiation level $Q_{ST,u}$ attained after a time long enough to discard transient dynamics (see Methods). We then interpret the discrepancies in $Q_{ST,u}$ across the simulations by relating them to the underlying graph topologies.

We observe strong differences in $Q_{ST,u}$ across graphs for varying m , and find that $\langle l \rangle$ explains at least 55% of the variation in $Q_{ST,u}$ across all graphs with $M = 7$ vertices for (Fig. 2.2b). Nonetheless, some specific graphs, such as the star graph, present higher levels of $Q_{ST,u}$ than expected by their average path length. To explain this discrepancy, we explore the effect of homogeneity in vertex degree h_d , as we showed in Eq. (2.12) that it decreases population size, which should in turn increase $Q_{ST,u}$ by intensifying stochastic drift. We find that h_d explains 57% of the variation for low m (Fig. 2.2c). However, the fit remains similar after correcting for differences in population size (see Table S1), indicating that irregular graphs structurally amplify the isolation of populations. Unbalanced migration fluxes lead central vertices to host more individuals than allowed by their carrying capacity. This causes increased competition that results in a higher death rate, so that migrants have a lower probability of further spreading their trait. Highly connected vertices therefore behave as bottlenecks, increasing the isolation of peripheral vertices and consequently amplifying $Q_{ST,u}$.

We then evaluate the concurrent effect of $\langle l \rangle$ and h_d on $Q_{ST,u}$ with a multivariate regression model that we fit independently for low and high migration regimes (Fig. 2.2d). The multivariate regression model explains at least 70% of the variation in $Q_{ST,u}$ for the migration regimes considered and for graphs with $M = 7$ vertices (see Table S2 for details). Moreover, we find that $\langle l \rangle$ and h_d have akin contributions to neutral differentiation for low m , but the effect of $\langle l \rangle$ increases for higher migration regimes while the effect of h_d decreases. To ensure that these conclusions can be generalised to larger graphs, we conduct the same analysis on a subset of graphs with $M = 9$ vertices and find congruent results (Fig. S1). In the absence of selection and with competitive interactions, graphs with a high average path length $\langle l \rangle$ and low homogeneity in vertex degree h_d , or similarly graphs with low connectivity and high heterogeneity in connectivity, show high levels of neutral differentiation.

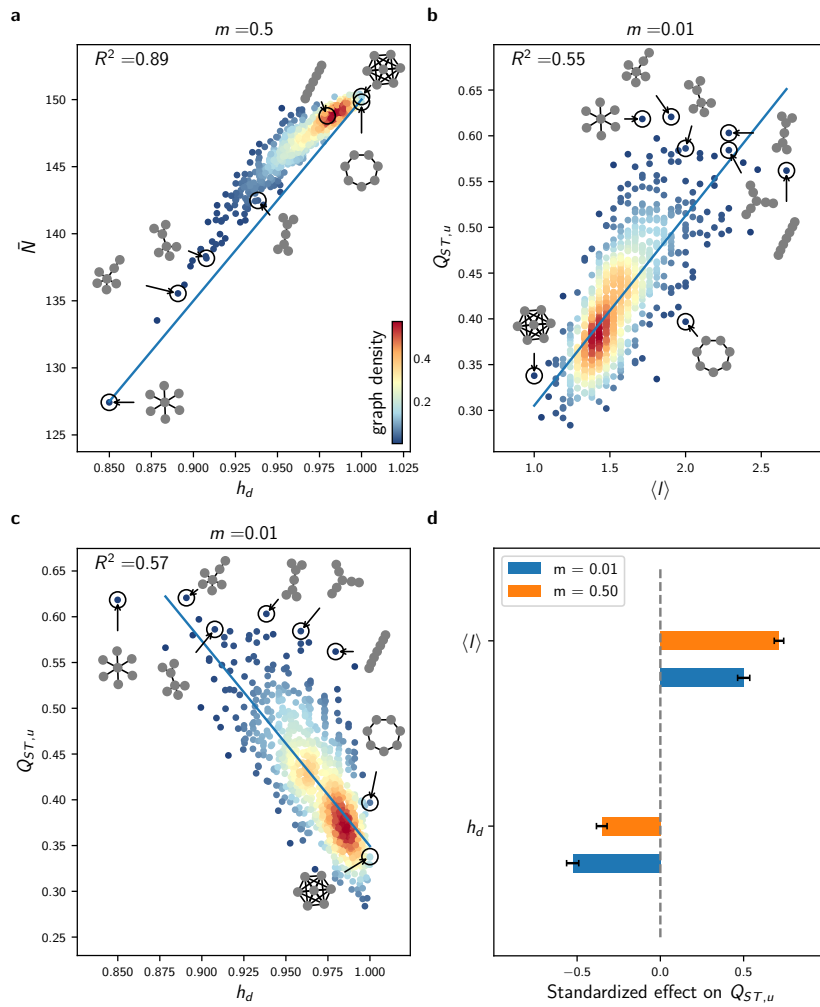


Fig. 2.2: Effect of $\langle l \rangle$ and h_d on average population size \bar{N} and neutral differentiation $Q_{ST,u}$ in the setting with no selection. (a) Response of \bar{N} to homogeneity in degree $h_d = \langle \sqrt{k} \rangle^2 / \langle k \rangle$ for all undirected connected graphs with $M = 7$ vertices and $m = 0.5$. (b) Response of $Q_{ST,u}$ to average path length $\langle l \rangle$ for similar simulations obtained with $m = 0.01$. (c) Response of $Q_{ST,u}$ to homogeneity in degree h_d for the same data. In (a), (b) and (c), each dot represents average results from 5 replicate simulations of the IBM, the colour scale corresponds to the proportion of the graphs with similar x and y axis values (graph density), and the blue line corresponds to a linear fit. (d) Standardized effect of h_d and $\langle l \rangle$ on $Q_{ST,u}$, obtained from multivariate regression models independently fitted on similar data obtained for $m = 0.01$ and $m = 0.5$. The contributions of $\langle l \rangle$ and h_d to $Q_{ST,u}$ are alike for low migration regimes. Error bars show 95% confidence intervals. Analogous results on graphs with $M = 9$ vertices are presented in Fig. S1 and all regression details can be found in Table S2.

2.2.4 Deterministic approximation of the population dynamics and adaptation under heterogeneous selection

We next consider heterogeneous selection and investigate the response of adaptive differentiation to the spatial distribution of habitat types, denoted as the Θ -spatial distribution. Adaptive differentiation emerges from local adaptation, but migration destabilises adaptation as a result of the influx of maladaptive migrants. We expect that higher connectivity between vertices of similar habitat type increases the level of adaptive differentiation, because it increases the proportion of well-adapted migrants. Local adaptation can be investigated by approximating the stochastic dynamics of the trait distribution with a deterministic partial differential equation (PDE). We demonstrate under mean field assumption how the deterministic approximation can be reduced to an equivalent two-habitat model. We analyse the reduced model with the theory of adaptive dynamics [36, 41] and find a critical migration threshold m^* that determines local adaptation. m^* depends on a quantity coined the habitat assortativity r_Θ , and we demonstrate with numerical simulations that r_Θ determines the overall adaptive differentiation level $Q_{ST,s}$ reached at steady state in the deterministic approximation.

Heterogeneous selection, captured by the dependence of the birth rate on Θ_i , generates a stabilising force that dampens the stochastic fluctuations of the adaptive trait distribution. The dynamics of the adaptive trait distribution consequently shows a deterministic behavior and we demonstrate in the Supplementary Note and Figs. S3 and S4 that the number of individuals on v_i with traits $s \in \Omega \subset \mathcal{S}$ can be approximated by the quantity $\int_\Omega n^{(i)}(s)ds$, where $n^{(i)}$ is a continuous function solution of the PDE

$$\partial_t n_t^{(i)}(s) = n_t^{(i)}(s) \left[b^{(i)}(s)(1 - m) - \frac{1}{K} \int_S n_t^{(i)}(\mathbf{s})d\mathbf{s} \right] + m \sum_{j \neq i} b_j(s) \frac{a_{i,j}}{d_j} n_t^{(j)}(s) + \frac{1}{2} \mu \sigma_\mu^2 \Delta_s \left[b^{(i)}(s) n_t^{(i)}(s) \right] \quad (2.4)$$

Equation (2.4) is similar to Eq. (2.3), except that it incorporates an additional term corresponding to mutation processes and that the birth rate is trait dependent. We show how Eq. (2.4) can be reduced to an equivalent two-habitat model under mean field assumption. The mean field approach differs slightly from the setting with no selection because vertices are labelled with Θ_i . Here we assume that vertices with similar habitat types have an equivalent position on the graph (see Fig. S5 for a graphical representation), so that all vertices with habitat type \bullet are characterised by the identical adaptive trait distribution that we denote by \bar{n}^\bullet , and are associated with the birth rate $b^\bullet(s) = b(1 - p(s - \theta_\bullet)^2)$. Let $P(\bullet, \bullet)$ denote the proportion of edges connecting a vertex v_i of type \bullet to a vertex v_j of type \bullet , and let $P(\bullet)$ denote the proportion of vertices v_i of type \bullet . By further assuming that habitats

are homogeneously distributed on the graph so that $P(\bullet) = P(\bullet) = \frac{1}{2}$, Eq. (2.4) transforms into

$$\begin{aligned}\partial_t \bar{n}_t^\bullet(s) &= \bar{n}_t^\bullet(s) \left[b^\bullet(s)(1-m) - \frac{1}{K} \int_S \bar{n}_t^\bullet(\mathbf{s}) d\mathbf{s} \right] + \frac{1}{2} \mu \sigma_\mu^2 (\Delta_s b^\bullet \bar{n}_t^\bullet)(s) \\ &\quad + \frac{m}{2} [(1-r_\Theta)b^\bullet(s)\bar{n}_t^\bullet(s) + (1+r_\Theta)b^\bullet(s)\bar{n}_t^\bullet(t)]\end{aligned}\quad (2.5)$$

(see Methods), where we define

$$r_\Theta = 2(P(\bullet, \bullet) - P(\bullet, \bullet)) \quad (2.6)$$

as the habitat assortativity of the graph, which ranges from -1 to 1 . When $r_\Theta = -1$, all edges connect dissimilar habitat types (disassortative graph), while as r_Θ tends towards 1 the graph is composed of two clusters of vertices with identical habitat types (assortative graph). Eq. (2.5) can be analysed with the theory of adaptive dynamics [36, 38, 41], a mathematical framework that provides analytical insights by assuming a trait substitution process. Following this assumption, the mutation term in Eq. (2.5) is omitted and the phenotypic distribution results in a collection of discrete individual types that are gradually replaced by others until evolutionary stability is reached (see Methods and [36, 38, 41] for details). By applying the theory of adaptive dynamics, we find a critical migration rate m^*

$$m^* = \frac{1}{(1-r_\Theta)} \frac{4p\theta^2}{(1+3p\theta^2)} \quad (2.7)$$

so that when $m > m^*$, a single type of individual exists with adaptive trait $s^* = (\theta_\bullet + \theta_\bullet)/2 = 0$ in the steady state (see Methods for the derivation of Eq. (2.7)). In this case, adaptive differentiation $Q_{ST,s}$ is nil and the average population size is given by $\bar{N} = bK(1-p\theta)^2$. In contrast, when $m = 0$ and/or $r_\Theta = 1$, all individuals are locally well-adapted with trait Θ_i on v_i , and it follows that the average population size is higher and equal to $\bar{N} = bK$, while adaptive differentiation is maximal and equal to $Q_{ST,s} = \text{Var}(\Theta)/(\text{Var}(\Theta)+0) = 1$. When $0 < m < m^*$, the coexistence of two types of individuals on each vertex v_i is predicted but the calculation of the trait values is more subtle. To understand the effect of m and r_Θ on the local trait distributions and on $Q_{ST,s}$, we therefore leave behind the adaptive dynamics framework and numerically solve Eq. (2.5) by including the mutation term. When $0 < m < m^*$, the local trait distributions are bimodal with peaks corresponding to the two types of individuals predicted by the adaptive dynamics. The highest peak corresponds to the well-adapted individuals, whose adaptation is destabilised by the influx of maladaptive migrants (Fig. 2.3a). This phenomenon is dampened as r_Θ increases, since the proportion of maladaptive migrants is reduced in assortative graphs (Fig. 2.3b). As a consequence, the habitat assortativity r_Θ increases the differentiation $Q_{ST,s}$ when $0 < m < m^*$ (Fig. 2.3c). The simulations further confirm that the adaptive dynamics prediction given by Eq. (2.7) is still valid when the continuous accumulation of mutations is considered, so that for $m > m^*$ the local trait distributions obtained from Eq. (2.5) are unimodal and $Q_{ST,s}$ vanishes (Fig. 2.3a,c). Our analysis of the mean field deterministic approximation Eq. (2.5) therefore demonstrates that assortative graphs present high levels of adaptive differentiation

$Q_{ST,s}$. On the other hand, the analysis shows that $Q_{ST,s}$ rapidly declines with increasing m on disassortative graphs, until $Q_{ST,s}$ vanishes when $m > m^*$.

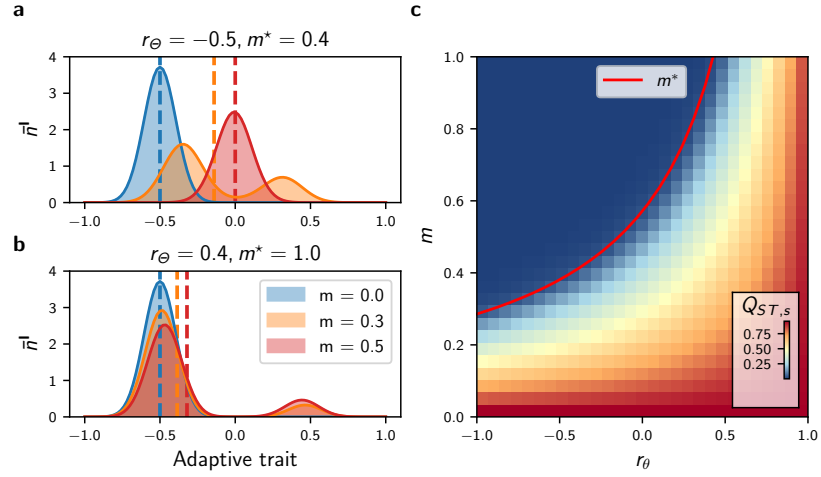


Fig. 2.3: Effect of habitat assortativity r_Θ and migration m on the local adaptive trait distribution \bar{n}^* and on the adaptive differentiation level $Q_{ST,s}$ under the mean field, deterministic approximation Eq. (2.5). (a) Effect of m and r_Θ on \bar{n}^* . Migration induces the apparition of maladaptive individuals (centred around $\theta_+ = 0.5$), which destabilise local adaptation by displacing the mean value of the well-adapted individuals (centred around $\theta_- = -0.5$). Together with the decrease in local adaptation, migration causes a displacement of the mean value of the local trait distribution (represented by the vertical dashed lines), which decreases local population size and adaptive differentiation $Q_{ST,s}$. (b) Similar data for higher r_Θ . Increasing r_Θ increases population size and $Q_{ST,s}$. (c) Effect of r_Θ on $Q_{ST,s}$. The red line indicates the critical migration threshold m^* predicted by Eq. (2.7); $Q_{ST,s}$ vanishes when $m > m^*$.

2.2.5 Effect of graph topology on adaptive differentiation under heterogeneous selection

To generalise the conclusions drawn from the mean field deterministic approximation Eq. (2.5), we generate different Θ -spatial distributions for varying graph topology, and compare outputs of the IBM simulations with those of Eq. (2.5) (see Methods for the details of the simulations). For each combination of Θ -spatial distribution and graph, we compute the habitat assortativity r_Θ , since r_Θ can be generalised from Eq. (2.6) to any graph topology following the original definition of [51] as

$$r_\Theta = \frac{\text{Cov}(\Theta_x, \Theta_\wedge)}{\sigma_{\Theta_x} \sigma_{\Theta_\wedge}} \quad (2.8)$$

where Θ_x and Θ_\wedge denote the sets of habitats found at the toe and tip of each directed vertex of graph V , and $\langle \Theta_x \rangle, \langle \Theta_\wedge \rangle$ and $\sigma_{\Theta_x}, \sigma_{\Theta_\wedge}$ denote their respective means and standard deviations (see Supplementary Note). The mean field deterministic approximation Eq. (2.5) is in

very good agreement with the IBM simulations for general graph ensembles at low migration regimes, and captures the response of \bar{N} and $Q_{ST,s}$ to r_Θ (Fig. 2.4). Nonetheless, under high migration regimes, higher levels of $Q_{ST,s}$ are observed in the stochastic simulations compared with the mean field deterministic approximation (Fig. S6). We hypothesize that this reinforcement is generated by stochastic drift, which must become the main driver of differentiation when local adaptation is lost for $m > m^*$, and perform a multivariate regression analysis to investigate the additional effect of $\langle l \rangle$ and h_d on $Q_{ST,s}$. As expected, the analysis highlights that the effect of $\langle l \rangle$ and h_d are substantial and complement the effect of r_Θ for high m (Fig. 2.5c for graphs with $M = 7$ vertices and Fig. S7a for $M = 9$), further explaining the discrepancies observed (see Table S3).

We extend our analyses to realistic landscapes with a continuum of habitat types by running simulations on graphs obtained from real spatial habitat datasets and by considering mean annual temperature as a proxy for habitat type (see Fig. S8 and Table S4). We also consider simulations accounting for trait-dependent competition to test whether our results hold under more complex ecological processes (see Supplementary Note for the implementation details and Table S5 for the results). The simulations are congruent and show that the effects of r_Θ , h_d and $\langle l \rangle$ are similar under these alternative settings, underlining the robustness of these metrics and the generality of our conclusions. Taken together, these results indicate that under sufficiently strong selection and sufficiently high habitat heterogeneity, adaptive differentiation $Q_{ST,s}$ is mainly driven by habitat assortativity r_Θ . Nonetheless, local adaptation is lost in disassortative graphs when $m > m^*$, such that $\langle l \rangle$ and h_d become complementary determinants of $Q_{ST,s}$ for high migration regimes.

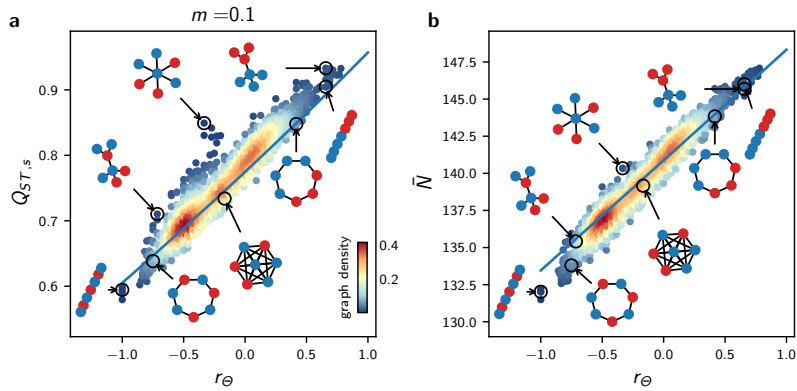


Fig. 2.4: Effect of habitat heterogeneity r_Θ on $Q_{ST,s}$ and average population size \bar{N} for general graph ensembles. (a) Effect of r_Θ on $Q_{ST,s}$ for all undirected connected graphs with $M = 7$ vertices and varying r_Θ , for $m = 0.1$. (b) Effect of r_Θ on average population size \bar{N} for the same simulations. In (a) and (b), each dot represents average results from 5 replicate simulations of the IBM, the colour scale corresponds to the proportion of the graphs with similar x and y axis values (graph density), and the blue lines correspond to results obtained from the mean field approximation Eq. (2.5). Insights from Eq. (2.5) are congruent with the IBM simulations for complex habitat connectivity patterns at low m . Similar results with $m = 0.5$ are presented in Fig. S6.

2.2.6 Effect of habitat assortativity on neutral differentiation under heterogeneous selection

We finally consider a setting with heterogeneous selection where individuals carry both neutral and adaptive traits. With distinct habitat types, selection promotes neutral differentiation by reducing the birth rate of maladaptive migrants, reinforcing the isolation of local populations. We have shown above that adaptive differentiation $Q_{ST,s}$ is driven by habitat assortativity r_Θ , so we expect r_Θ , together with the topological metrics found in the setting with no selection, to influence the level of neutral differentiation $Q_{ST,u}$. We first investigate how the response of $Q_{ST,u}$ to migration compares between the setting with no selection and the setting with heterogeneous selection for graphs with an identical topology. We then examine how the response compares between graphs with an identical topology but different r_Θ . We finally consider simulations on different graphs with varying r_Θ to assess the concurrent effect of $\langle l \rangle$, h_d and r_Θ on $Q_{ST,u}$.

Migration has a fitness cost because maladaptive migrants present lower fitness. Under an equivalent migration regime, migrants therefore have a lower probability of reproduction, increasing the populations' isolation compared with a setting without selection. Simulations with varying m on the complete graph confirm that selection in heterogeneous habitats reinforces $Q_{ST,u}$ compared with a setting without selection (Fig. 2.5a). Nonetheless, previous results show that adaptive differentiation $Q_{ST,s}$ vanishes on a disassortative graph when $m > m^*$, implying that individuals become equally fit in all habitats. In this case, the isolation effect of heterogeneous selection is lost and $Q_{ST,u}$ reaches a similar level as in the setting with no selection for $m > m^*$ (Fig. 2.5a), although $Q_{ST,u}$ is slightly higher in the setting with heterogeneous selection due to a lower population size ($\bar{N} = bK(1 - p\theta)$ vs. $\bar{N} = bK$, see section above and Methods). This suggests that r_Θ reinforces $Q_{ST,u}$, as assortative graphs sustain higher levels of adaptive differentiation (Figs. 2.3 and 2.4). Simulations on the path graph with varying Θ -spatial distribution support this conclusion for high migration regimes, but show the opposite relationship under low migration regimes, where the habitat assortativity r_Θ decreases $Q_{ST,u}$ (Fig. 2.5b). Assortative graphs are composed of large clusters of vertices with similar habitats, within which migrants can circulate without fitness losses. Local neutral trait distributions become more correlated within these clusters, resulting in a decline in $Q_{ST,u}$ for assortative graphs compared with disassortative graphs. Figure 2.5b therefore highlights the ambivalent effect of r_Θ on $Q_{ST,u}$. r_Θ reinforces $Q_{ST,u}$ by favouring adaptive differentiation, but also decreases $Q_{ST,u}$ by decreasing population isolation within clusters of vertices with the same habitat type.

We compare the effect of r_Θ on $Q_{ST,u}$ to the effect of the topology metrics $\langle l \rangle$ and h_d found in the setting with no selection using a multivariate regression analysis on simulation results obtained for different graphs with varying Θ -spatial distribution (Fig. 2.5d for graphs with $M = 7$ vertices and Fig. S7b for $M = 9$). The multivariate model explains the discrepancies in $Q_{ST,u}$ across the simulations for low and high migration regimes (see Table S3 for details), and we find that r_Θ , $\langle l \rangle$ and h_d contribute similarly to neutral differentiation. Hence, the effects of r_Θ and the topology metrics $\langle l \rangle$ and h_d add up under heterogeneous

selection. A change in sign of the standardized effect of r_Θ on $Q_{ST,s}$ for low and high migration regimes verifies that the ambivalent effect of r_Θ on $Q_{ST,u}$ found on the path graph holds for general graph ensembles. Simulations with trait-dependent competition and simulations on realistic graphs with a continuum of habitat types equally confirm the ambivalent effect of r_Θ and further support the complementary effect of $\langle l \rangle$ and h_d on $Q_{ST,u}$ (see Fig. S8). $\langle l \rangle$ and h_d therefore drive neutral differentiation with and without heterogeneous selection. r_Θ becomes an additional determinant of neutral differentiation under heterogeneous selection. In contrast to the non-ambivalent, positive effect of habitat assortativity on adaptive differentiation, r_Θ can amplify or depress neutral differentiation depending on the migration regime considered.

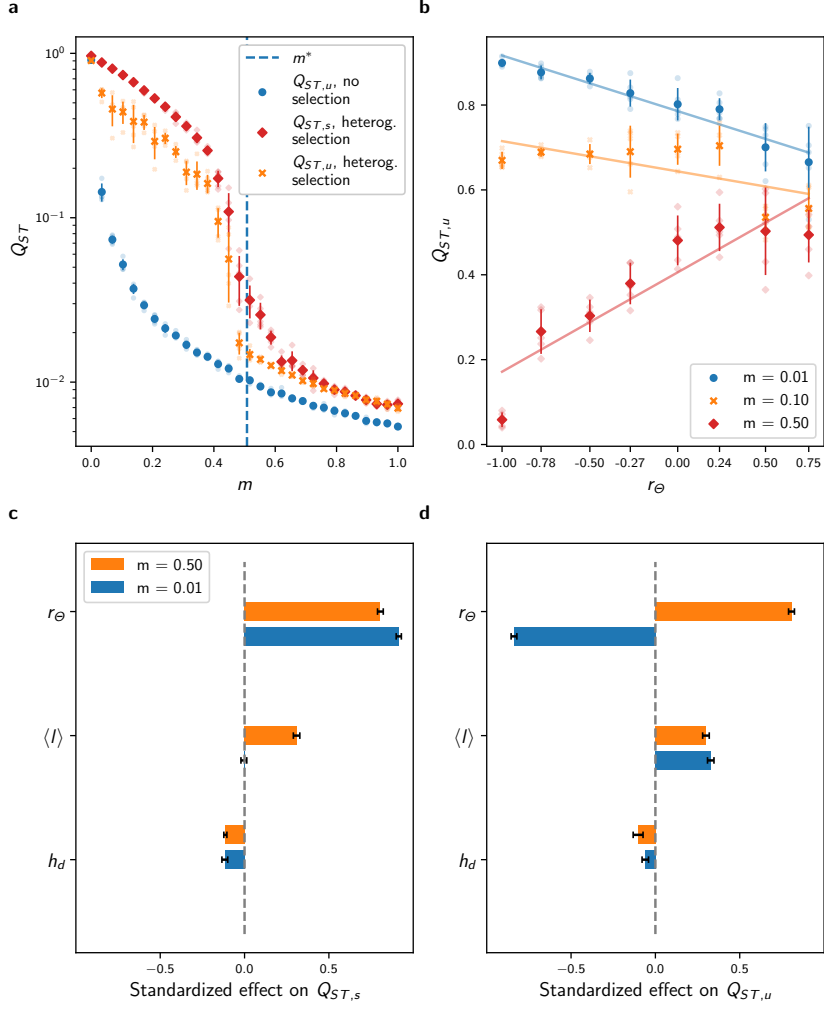


Fig. 2.5: Effect of r_Θ , $\langle l \rangle$ and h_d on $Q_{ST,s}$ and $Q_{ST,u}$ in the setting with heterogeneous selection. (a) Comparison of the response of $Q_{ST,u}$ to migration with the response of $Q_{ST,u}$ in the setting with no selection for the complete graph. The dashed vertical blue line corresponds to the critical migration regime m^* predicted by Eq. (2.7). Heterogeneous selection increases $Q_{ST,u}$ when $m < m^*$, but local adaptation is lost when $m > m^*$, and in this case $Q_{ST,u}$ reaches similar levels as $Q_{ST,u}$ in the setting with no selection. (b) Response of $Q_{ST,u}$ to r_Θ and migration for the path graph. r_Θ correlates positively with $Q_{ST,u}$ for high m , but correlates negatively for low m . In (a–b), each plain dot represents average results from 5 replicate simulations, the bars represent one standard deviation, and each fade dot represents a single replicate value. (c–d) Standardized effect of h_d , $\langle l \rangle$ and r_Θ on $Q_{ST,s}$ and $Q_{ST,u}$ obtained from a multivariate regression model independently fitted for low and high migration regimes on average results from 5 replicate simulations of the IBM on all undirected connected graphs with $M = 7$ vertices and varying r_Θ (see Methods). The ambivalence of the effect of r_Θ on $Q_{ST,u}$ found for the path graph holds for general graph ensembles and adds up to that of $\langle l \rangle$ and h_d . Error bars show 95% confidence intervals. Analogous results on graphs with $M = 9$ vertices are presented in Fig. S7 and all regression details can be found in Table S3.

2.3 Discussion

Using analytical tools and simulations, we have built upon a graph representation of landscapes and a stochastic individual-based model to investigate how landscape features drive phenotypic differentiation. Our study is based on a first principles modelling approach [29] describing the stochastic dynamics of individuals and capturing the interplay between population dynamics, phenotypic evolution and spatial dynamics in heterogeneous habitats. In contrast to metacommunity models [17, 18, 19, 20, 21, 22, 23] and evolutionary metacommunity models [26, 27], we have focused on differentiation at the population level. Quantitative genetics and population genetics studies have investigated the effect of topology on differentiation under the assumption of non-overlapping generations, constant population sizes and regular spatial structures [31, 48, 33, 34, 52]. Generalising beyond these assumptions, our modelling framework accounts for population dynamics and includes competition and frequency-dependent selection. The systematic investigation of the effect of topology on differentiation over general graph ensembles and under different ecological settings shows that average path length $\langle l \rangle$, homogeneity in vertex degree h_d and habitat assortativity r_Θ contribute equally to differentiation. These results support correlative studies that have associated population differentiation [44, 53] and species richness [54, 4, 55, 56, 57, 58, 5, 59] with a variety of metrics used as surrogates for connectivity, connectivity heterogeneity and habitat heterogeneity. To further our understanding of the origin of spatial biodiversity patterns, the contribution of landscape properties to discrepancies in population differentiation could be investigated at large scales by (i) using techniques to project real landscapes on graphs (see Fig. S8a–b); (ii) characterising the landscape features with $\langle l \rangle$, h_d and r_Θ ; and (iii) relating the obtained metrics maps to observation data. More generally, the proposed eco-evolutionary model on spatial graphs could be combined with approximate bayesian computation to estimate ecological, spatial and evolutionary processes of real populations from observation data, similarly to [60]. This approach might improve current inferential techniques based on models that do not account for competition nor heterogeneous selection (see e.g. [61]). Overall, our results point to topology metrics that can connect spatial biodiversity patterns to the generating eco-evolutionary and spatial processes.

In the absence of selection, neutral differentiation is more pronounced on graphs with a high average path length $\langle l \rangle$, but is also negatively associated with homogeneity in degree h_d (Fig. 2.2c–d). $\langle l \rangle$ generalises the concept of dimensionality in [48, 33, 34], where it is shown that differentiation is lower for two-dimensional grid graphs compared with path graphs. $\langle l \rangle$ also closely relates to the concept of resistance distance shown theoretically and empirically to drive genetic differentiation [62, 53]. At the species level, a similar effect of $\langle l \rangle$ on β -diversity (pairwise differences in species composition) has been reported with the graph metacommunity model of [21] and with the graph eco-evolutionary metacommunity model of [26]. Accounting for population dynamics and specifically including competition processes,

we have shown that not only $\langle l \rangle$ but also h_d affects neutral phenotypic differentiation (Fig. 2.2c,d). Our model realistically assumes that population growth is limited by the local carrying capacity. The latter becomes saturated on highly connected vertices in irregular graphs, an effect that has been experimentally documented in microcosm experiments [63]. As a consequence, central vertices behave as bottlenecks and amplify the isolation of peripheral vertices [13]. The role of h_d cannot be captured with classical metapopulation and quantitative genetics models or with models of evolutionary dynamics in graphs, as they assume constant population size. This behaviour should be prevalent in patchy landscapes where interspecific competition is high because of limiting resources. Our study highlights that heterogeneity in connectivity can reinforce differentiation patterns through the creation of unbalanced migration fluxes which affect ecological equilibrium.

Habitat assortativity r_Θ is a useful indicator for assessing how the spatial distribution of habitat types modulates local adaptation and adaptive differentiation in complex landscapes [64]. While adaptation has been extensively studied along environmental gradients [65, 32, 66, 67, 40, 68, 35], landscapes can be patchy and it is unrealistic to assume regularity [16]. Our model of heterogeneous selection on spatial graphs extends the two-habitat setting investigated in [36, 52, 38, 41] and captures irregularity in connectivity between distinct habitats [16]. Similarly to the aforementioned studies, we have found a critical migration regime m^* that dictates the possibility of adaptation. Equation (2.7) indicates that m^* increases with increasing selection strength p and with increasing environmental heterogeneity θ , the latter playing a similar role as the slope of the environmental gradient in [65, 32, 67, 40]. Local adaptation would consequently be sustained under higher migration regimes following an increase in these parameters. Additionally, the critical migration regime m^* in Eq. (2.7) involves the habitat assortativity r_Θ , which must be regarded as a measure of habitat spatial auto-correlation based on the dispersal range of a species [64]. Our results indicate that for general habitat distributions, r_Θ is the main determinant of adaptive differentiation under sufficiently strong selection p and high habitat heterogeneity θ , irrespective of the graph topology (Fig. 2.5c, Fig. S7a and Fig. S8). As p decreases, however, the effect of stochastic drift on $Q_{ST,s}$ should increase, and in this case the topology metrics $\langle l \rangle$ and h_d should become the most important determinants of $Q_{ST,s}$. Our results predict that in landscapes with heterogeneous habitats and where selection is strong, populations structured over assortative habitats are larger, support higher adaptive differentiation, and can be locally well-adapted even in the case where migration rates are high.

Spatial eco-evolutionary feedbacks in heterogeneous habitats can critically affect differentiation [64]. While most eco-evolutionary studies have investigated diversification by considering a unique adaptive trait [35, 66, 67, 40], distinguishing between neutral and adaptive processes is crucial [9] and our work underlines the distinct responses of neutral and adaptive differentiation to landscape features (Fig. 2.5c vs. Fig. 2.5d). Our study builds upon recent mathematical models that consider the co-evolution of neutral and adaptive traits [42, 43] and extends those works to a spatial context. Our work provides an analytical framework to the concept of isolation by environment (IBE) [13], which has been suggested to be one of the most important mechanisms governing differentiation in nature [14]. Heterogeneous selection leads to more isolation by modifying the fitness of migrants [40],

which further reduces gene flow [64] and therefore affects the level of neutral differentiation (Fig. 2.5a) [15]. Our work proposes a mechanism by which habitat assortativity, relative to the migration regime, controls the direction of the effect of habitat heterogeneity on differentiation (Fig. 2.5d). Patchy, heterogeneous habitats can promote neutral differentiation as a result of selection that reduces effective migration [59]. Nonetheless, adaptive differentiation decreases substantially when migration is high relative to the critical migration regime m^* . In this case, neutral differentiation should be higher in landscapes with more aggregated habitats [64]. Our study suggests that habitat assortativity must be considered for a complete understanding of differentiation in complex environments [59].

In conclusion, we have established how differentiation can emerge at the population level from eco-evolutionary feedbacks in complex landscapes by using an analytical description of micro-evolutionary processes explicitly accounting for spatial dynamics over graphs. Our study formalises how differentiation emerges from the interplay between spatial dynamics, the co-evolution of neutral and adaptive traits, and landscape properties. Connectivity and habitat assortativity emerge as core determinants of differentiation in spatial graphs. These results resonate with empirical findings and previous theoretical works. Our study further stresses that habitat assortativity can depress or foster neutral differentiation depending on the migration regime. Additionally, our work highlights that heterogeneity in connectivity is an equally strong determinant of differentiation because highly connected habitats behave as bottlenecks, increasing the isolation of peripheral habitats. The present approach offers a promising framework for studying complex adaptive systems, as it can elucidate how macroscopic properties emerge from microscopic processes acting upon agents structured over complex spatio-evolutionary structures.

2.4 Methods

2.4.1 Mean field approximation

In the setting with no selection, the mean field approach involves the assumption that all vertices having the same degree are equivalent. For this, let $P(k, k')$ denote the proportion of edges that map a vertex with degree k to a vertex with degree k' , and consider the average population size $\bar{N}_t^{(k)}$ in each vertex with degree k at time t . An individual has probability $P(k, k')/k'$ to migrate from a vertex with degree k' to a vertex with degree k . Viewing $a_{i,j}/d_j$ as the probability that an individual on v_i chosen for migration moves to v_j , Eq. (2.3) then transforms into

$$\partial_t \bar{N}_t^{(k)} = \bar{N}_t^{(k)} \left[b(1 - m) - \frac{\bar{N}_t^{(k)}}{K} \right] + mbk \sum_{k' \in V} \frac{P(k, k')}{k'} \bar{N}_t^{(k')} \quad (2.9)$$

Assuming uncorrelated graphs for which $P(k,k')/k' = P(k')/\langle k \rangle$, where $\langle k \rangle$ denotes the average degree of the graph [49], yields

$$\partial_t \bar{N}_t^{(k)} = \bar{N}_t^{(k)} \left[b(1-m) - \frac{\bar{N}_t^{(k)}}{K} \right] + mb \frac{k}{\langle k \rangle} \bar{N}_t \quad (2.10)$$

where

$$\bar{N}_t = \sum_k P(k) \bar{N}_t^{(k)}. \quad (2.11)$$

When solving for the stationary state and setting $m = 1$, one obtains $\bar{N}^{(k)} = \sqrt{bK \frac{k}{\langle k \rangle}} \bar{N}$ from Eq. (2.10). Combining this with Eq. (2.11) yields

$$\bar{N} = bK \langle \sqrt{k} \rangle^2 / \langle k \rangle \quad (2.12)$$

In the setting with heterogeneous selection, the mean field approach involves the assumption that all vertices with a similar habitat are equivalent. In this case, an individual from a vertex of habitat type \bullet has the probability $P(\bullet, \bullet)/P(\bullet)$ of migrating to a vertex of type \bullet , and therefore Eq. (2.4) transforms into

$$\begin{aligned} \partial_t \bar{n}_t^\bullet(s) &= \bar{n}_t^\bullet(s) \left[b^\bullet(s)(1-m) - \frac{1}{K} \int_S \bar{n}_t^\bullet(\mathbf{s}) d\mathbf{s} \right] + \frac{1}{2} \mu \sigma_\mu^2 \Delta_s [b^\bullet(s) \bar{n}_t^\bullet(s)] \\ &\quad + m \sum_{i \in \{\bullet, \bullet\}} b_i(s) \frac{P(\bullet, i)}{P(i)} \bar{n}_t^i(s) \end{aligned} \quad (2.13)$$

Considering that $P(\bullet) = P(\bullet) = \frac{1}{2}$ (habitats are equally distributed), $P(\bullet, \bullet) + P(\bullet, \bullet) = P(\bullet)$ (sum of conditional expectations), and $r_\Theta = 2(P(\bullet, \bullet) - P(\bullet, \bullet))$ (Eq. (2.6)), one obtains

$$P(\bullet, \bullet) = \frac{1}{4}(1 - r_\Theta) \quad \text{and} \quad P(\bullet, \bullet) = \frac{1}{4}(1 + r_\Theta) \quad (2.14)$$

Combining Eq. (2.14) with Eq. (2.13) yields Eq. (2.5). We show in the Supplementary Note how one can derive Eq. (2.6) from the general definition of assortativity given in Eq. (2.8) and initially introduced in [51].

2.4.2 Adaptive dynamics on graphs

The adaptive dynamics theory considers a monomorphic population that evolves following a trait substitution process [36]. Accordingly, the trait s of the monomorphic metapopulation evolves gradually along the direction given by its fitness gradient, until it reaches a singular strategy s^* for which the fitness gradient vanishes. By omitting the mutation term, Eq. (2.6) can be written in the matrix form

$$\partial_t \bar{\mathbf{n}}_t(s) = M(s, \bar{\mathbf{N}}_t) \bar{\mathbf{n}}_t(s) \quad (2.15)$$

where $\bar{\mathbf{n}}_t = (\bar{n}_t^\bullet, \bar{n}_t^\bullet)$ and $\bar{\mathbf{N}}_t = (\bar{N}_t^\bullet, \bar{N}_t^\bullet)$ are the vectors containing the population densities and the population size on each habitat type, and

$$M(s, \bar{\mathbf{N}}) = \begin{bmatrix} \mathfrak{r}^\bullet(s, \bar{N}^\bullet) & \frac{m}{2}(1 - r_\Theta)b^\bullet(s) \\ \frac{m}{2}(1 - r_\Theta)b^\bullet(s) & \mathfrak{r}^\bullet(s, \bar{N}^\bullet) \end{bmatrix} \quad (2.16)$$

is the so-called projection matrix [36], with $\mathfrak{r}^\bullet(s, \bar{N}^\bullet) = b^\bullet(s)(1 + \frac{m}{2}(r_\Theta - 1)) - \bar{N}^\bullet/K$. The overall fitness of individuals with trait s is the leading eigenvalue of M , which we denote with $\lambda(s, \bar{\mathbf{N}})$. We obtain the singular strategy s^* by setting the fitness gradient $\frac{\partial \lambda}{\partial s}(s, \bar{\mathbf{N}}) = 0$, from which we further obtain the demographic equilibrium \bar{N}^{s^*} . Because of symmetries, we must have $\bar{N}^{\bullet, s^*} = \bar{N}^{\bullet, s^*}$ and $s^* = \frac{\theta_\bullet + \theta_\bullet}{2} = 0$, such that $\bar{N}^{\bullet, s^*} = \bar{N}^{\bullet, s^*} = bK(1 - p\theta^2)$. s^* is said to be evolutionary stable if no mutants can invade, i.e. if s^* locally maximises the fitness of a mutant with trait y in the resident population with trait s^* , given by $\lambda(y, \bar{\mathbf{N}}^{s^*})$ (see [36] for details). One can show that $\left[\frac{\partial \lambda}{\partial y}(y, \bar{\mathbf{N}}^{s^*}) \right]_{y=s^*} = 0$ and the condition for evolutionary stability becomes $\left[\frac{\partial^2 \lambda}{\partial y^2}(y, \bar{\mathbf{N}}^{s^*}) \right]_{y=s^*} < 0$. We compute and simplify this inequality through computer algebra (see Mathematica notebook provided in the simulation code), which leads to Eq. (2.7).

2.4.3 Numerical simulations

The model was implemented in a multi-purpose Julia package called `EvoId.jl`, available at <https://github.com/vboussange/EvoId.jl>. For each result presented, $b = 1$, local carrying capacity $K = 150$, selection strength $p = 1$, mutation rate $\mu = 0.1$, mutation range $\sigma_\mu = 5 \cdot 10^{-2}$, and total time span $t = 1000$. This parameter choice made it possible to discard transient dynamics while obtaining results in a reasonable computational time (see Fig. S9). In settings (1) and (2), we ran simulations on all of the 853 undirected connected graphs with $M = 7$ vertices and on 1126 of the 261,080 undirected connected graphs with $M = 9$ vertices, listed at <http://oeis.org/A001349>. Graphs with $M = 9$ vertices were selected with a stratified sampling method: we randomly sampled without replacement a maximum of 50 graphs for each class of graphs with an equal number of vertices. For the setting with heterogeneous selection, we generated the labeled graphs by randomly generating Θ -spatial distributions, and by using a stratified sampling strategy to select without replacement at most 3 and 2 Θ -spatial distributions corresponding to the quartiles of the r_θ values obtained, respectively for graphs with $M = 7$ and $M = 9$ vertices. This sampling strategy allowed to obtain a uniform distribution of the topology metrics investigated in the study, and therefore permitted to correctly represent the population of graphs to investigate their effect on differentiation. We then computed $Q_{ST,u}$ and $Q_{ST,s}$, which we further averaged over the last time steps and across the replicates. Since the dynamics of $Q_{ST,u}$ is characterised by large quadratic variations, we simulated individuals with $d = 300$ neutral traits, where each trait can independently be affected by mutations. $Q_{ST,u}$ values presented were then obtained from the average $Q_{ST,u}$ for each trait. This reduced the variance of the numerical simulations and is also biologically meaningful because populations are characterised by many traits, most of which are neutral [9]. As

initial conditions, MK individuals were homogeneously distributed over all of the vertices, with traits centred on 0 and with standard deviation σ_μ . Graph metrics used for the meta-analysis were calculated using the **LightGraphs.jl** library [69]. We numerically solved the PDEs with a finite difference scheme using **DifferentialEquations.jl** [70], ensuring that the domain was large enough to avoid border effects.

2.4.4 Statistics and reproducibility

Statistical analyses were conducted in Julia using **StatsKit.jl**. All simulations can be exactly reproduced from the code available at <https://github.com/vboussange/differentiation-in-spatial-graphs>.

Data availability

The data underlying our figures is available at <https://github.com/vboussange/differentiation-in-spatial-graphs>.

Code availability

The simulation code is available at <https://github.com/vboussange/differentiation-in-spatial-graphs>.

Author contributions

V.B. and L.P. designed research; V.B. performed research; V.B. and L.P. wrote the paper.

Acknowledgements

We thank Thomas Poulet, Sylvian Billiard, Sepideh Mirrahimi, Heike Lischke, Joshua Payne, Conor Waldock, Yaquan Chang, Flora Desmet, Benjamin Flück and Alexander Skeels for helpful discussions and comments on the manuscript. L.P. was supported by the Swiss National Science Foundation grant (N^o 310030_188550). We thank two anonymous reviewers for constructive comments and valuable suggestions on a previous version of this article.

References

- [1] S. P. Hubbell. *The unified neutral theory of biodiversity and biogeography*. Monographs in Population Biology 32. Princeton [etc]: Princeton University Press, 2001.
- [2] C. Rahbek et al. “Building mountain biodiversity: Geological and evolutionary processes”. In: *Science* 365.6458 (2019), pp. 1114–1119. DOI: 10.1126/science.aax0151.
- [3] W.-N. Ding et al. “Ancient orogenic and monsoon-driven assembly of the world’s richest temperate alpine flora”. In: *Science* 369.6503 (2020), pp. 578–581. DOI: 10.1126/science.abb4484.
- [4] M. S. Dias et al. “Global imprint of historical connectivity on freshwater fish biodiversity”. In: *Ecology Letters* 17.9 (2014). Ed. by M. Anderson, pp. 1130–1140. DOI: 10.1111/ele.12319.
- [5] J.-F. Guégan, S. Lek, and T. Oberdorff. “Energy availability and habitat heterogeneity predict global riverine fish diversity”. In: *Nature* 391.6665 (1998), pp. 382–384. DOI: 10.1038/34899.
- [6] S. A. Levin. “Complex adaptive systems: Exploring the known, the unknown and the unknowable”. In: *Bulletin of the American Mathematical Society* 40.01 (2002), pp. 3–20. DOI: 10.1090/S0273-0979-02-00965-5.
- [7] J. S. Cabral, L. Valente, and F. Hartig. “Mechanistic simulation models in macroecology and biogeography: state-of-art and prospects”. In: *Ecography* 40.2 (2017), pp. 267–280. DOI: 10.1111/ecog.02480.
- [8] S. Lion. “Moment equations in spatial evolutionary ecology”. In: *Journal of Theoretical Biology* 405 (2016), pp. 46–57. DOI: 10.1016/j.jtbi.2015.10.014.
- [9] R. Holderegger, U. Kamm, and F. Gugerli. “Adaptive vs. neutral genetic diversity: implications for landscape genetics”. In: *Landscape Ecology* 21.6 (2006), pp. 797–807. DOI: 10.1007/s10980-005-5245-9.
- [10] M. Slatkin. “Isolation by distance in equilibrium and non-equilibrium populations”. In: *Evolution* 47.1 (1993), pp. 264–279. DOI: 10.1111/j.1558-5646.1993.tb01215.x.
- [11] U. Dieckmann and M. Doebeli. “On the origin of species by sympatric speciation”. In: *Nature* 400.6742 (1999), pp. 354–357. DOI: 10.1038/22521.
- [12] N. L. Kaplan, R. Hudson, and C. H. Langley. “The hitchhiking effect revisited.” In: *Genetics* 123.4 (1989), pp. 887–899. DOI: 10.1093/genetics/123.4.887.

- [13] L. Orsini et al. “Drivers of population genetic differentiation in the wild: Isolation by dispersal limitation, isolation by adaptation and isolation by colonization”. In: *Molecular Ecology* 22.24 (2013), pp. 5983–5999. DOI: 10.1111/mec.12561.
- [14] I. J. Wang and G. S. Bradburd. “Isolation by environment”. In: *Molecular Ecology* 23.23 (2014), pp. 5649–5662. DOI: 10.1111/mec.12938.
- [15] D. Garant, S. E. Forde, and A. P. Hendry. “The multifarious effects of dispersal and gene flow on contemporary adaptation”. In: *Functional Ecology* 21.3 (2007), pp. 434–443. DOI: 10.1111/j.1365-2435.2006.01228.x.
- [16] M. R. Dale and M. Fortin. “From graphs to spatial graphs”. In: *Annual Review of Ecology, Evolution, and Systematics* 41 (2010), pp. 21–38. DOI: 10.1146/annurev-ecolsys-102209-144718.
- [17] M. D. Holland and A. Hastings. “Strong effect of dispersal network structure on ecological dynamics”. In: *Nature* 456.7223 (2008), pp. 792–794. DOI: 10.1038/nature07395.
- [18] L. J. Gilarranz and J. Bascompte. “Spatial network structure and metapopulation persistence”. In: *Journal of Theoretical Biology* 297 (2012), pp. 11–16. DOI: 10.1016/j.jtbi.2011.11.027.
- [19] L. Mari et al. “Metapopulation persistence and species spread in river networks”. In: *Ecology Letters* 17.4 (2014). Ed. by F. Jordán, pp. 426–434. DOI: 10.1111/ele.12242.
- [20] D. Gravel, F. Massol, and M. A. Leibold. “Stability and complexity in model meta-ecosystems”. In: *Nature Communications* 7.1 (2016), p. 12457. DOI: 10.1038/ncomms12457.
- [21] F. Carrara et al. “Dendritic connectivity controls biodiversity patterns in experimental metacommunities”. In: *Proceedings of the National Academy of Sciences of the United States of America* 109.15 (2012), pp. 5761–5766. DOI: 10.1073/pnas.1119651109.
- [22] P. L. Thompson, B. Rayfield, and A. Gonzalez. “Loss of habitat and connectivity erodes species diversity, ecosystem functioning, and stability in metacommunity networks”. In: *Ecography* 40.1 (2017), pp. 98–108. DOI: 10.1111/ecog.02558.
- [23] Y. Suzuki and E. P. Economo. “From species sorting to mass effects: spatial network structure mediates the shift between metacommunity archetypes”. In: *Ecography* (2021), p. 05453. DOI: 10.1111/ecog.05453.

- [24] F. Pelletier, D. Garant, and A. Hendry. “Eco-evolutionary dynamics”. eng. In: *Philosophical Transactions of the Royal Society of London. Series B, Biological Sciences* 364.1523 (2009), pp. 1483–1489. DOI: 10.1098/rstb.2009.0027.
- [25] J. Tkadlec et al. “Population structure determines the tradeoff between fixation probability and fixation time”. In: *Communications Biology* 2.1 (2019), p. 138. DOI: 10.1038/s42003-019-0373-y.
- [26] E. P. Economo and T. H. Keitt. “Species diversity in neutral metacommunities: a network approach”. In: *Ecology Letters* 11.1 (2007), 071117033013001–???. DOI: 10.1111/j.1461-0248.2007.01126.x.
- [27] E. P. Economo and T. H. Keitt. “Network isolation and local diversity in neutral metacommunities”. In: *Oikos* 119.8 (2010), pp. 1355–1363. DOI: 10.1111/j.1600-0706.2010.18272.x.
- [28] R. Muneepetarakul et al. “Neutral metacommunity models predict fish diversity patterns in MississippiMissouri basin”. In: *Nature* 453.7192 (2008), pp. 220–222. DOI: 10.1038/nature06813.
- [29] N. Champagnat, R. Ferrière, and S. Méléard. “Unifying evolutionary dynamics: From individual stochastic processes to macroscopic models”. In: *Theoretical Population Biology* 69.3 (2006), pp. 297–321. DOI: 10.1016/j.tpb.2005.10.004.
- [30] V. Bansaye and S. Méléard. “Some stochastic models for structured populations : scaling limits and long time behavior”. In: *Stochastic Models for Structured Populations: Scaling Limits and Long Time Behavior* (2015), pp. 1–107. DOI: 10.1007/978-3-319-21711-6. arXiv: 1506.04165.
- [31] R. Bürger. *The mathematical theory of selection, recombination, and mutation*. eng. Wiley series in mathematical and computational biology. Chichester [etc]: J. Wiley, 2000.
- [32] M. Slatkin. “Spatial patterns in the distributions of polygenic characters”. In: *Journal of Theoretical Biology* 70.2 (1978), pp. 213–228. DOI: 10.1016/0022-5193(78)90348-X.
- [33] R. Lande. “Isolation by distance in a quantitative trait”. In: *Genetics* 128.2 (1991), pp. 443–452.
- [34] T. Nagylaki. “Geographical variation in a quantitative character.” In: *Genetics* 136.1 (1994), pp. 361–81.
- [35] M. Doebeli and U. Dieckmann. “Speciation along environmental gradients”. In: *Nature* 421.6920 (2003), pp. 259–264. DOI: 10.1038/nature01274.

- [36] G. Meszéna, I. Czibula, and S. Geritz. “Adaptive Dynamics in a 2-Patch Environment: A Toy Model for Allopatric and Parapatric Speciation”. In: *Journal of Biological Systems* 05.02 (1997), pp. 265–284. DOI: 10.1142/S0218339097000175.
- [37] R. Aguilée, D. Claessen, and A. Lambert. “Adaptive radiation driven by the interplay of eco-evolutionary and landscape dynamics”. In: *Evolution* 67.5 (2012), no–no. DOI: 10.1111/evo.12008.
- [38] F. Débarre, O. Ronce, and S. Gandon. “Quantifying the effects of migration and mutation on adaptation and demography in spatially heterogeneous environments”. In: *Journal of Evolutionary Biology* 26.6 (2013), pp. 1185–1202. DOI: 10.1111/jeb.12132.
- [39] J. Wickman et al. “Determining selection across heterogeneous landscapes: A perturbation-based method and its application to modeling evolution in space”. In: *The American Naturalist* 189.4 (2017), pp. 381–395. DOI: 10.1086/690908.
- [40] J. Polechová. “Is the sky the limit? On the expansion threshold of a species’ range”. In: *PLoS Biology* 16.6 (2018), pp. 1–18. DOI: 10.1371/journal.pbio.2005372.
- [41] S. Mirrahimi and S. Gandon. “Evolution of specialization in heterogeneous environments: equilibrium between selection, mutation and migration”. In: *Genetics* 214.2 (2020), pp. 479–491. DOI: 10.1534/genetics.119.302868.
- [42] S. Billiard et al. “Stochastic dynamics of adaptive trait and neutral marker driven by eco-evolutionary feedbacks”. In: *Journal of Mathematical Biology* 71.5 (2015), pp. 1211–1242. DOI: 10.1007/s00285-014-0847-y. arXiv: 1310.6274.
- [43] N. Anceschi et al. “Neutral and niche forces as drivers of species selection”. In: *Journal of Theoretical Biology* 483 (2019), p. 109969. DOI: 10.1016/j.jtbi.2019.07.021.
- [44] S. Manel et al. “Landscape genetics: combining landscape ecology and population genetics”. In: *Trends in Ecology & Evolution* 18.4 (2003), pp. 189–197. DOI: 10.1016/S0169-5347(03)00008-9.
- [45] R. Lande. “NEUTRAL THEORY OF QUANTITATIVE GENETIC VARIANCE IN AN ISLAND MODEL WITH LOCAL EXTINCTION AND COLONIZATION”. In: *Evolution* 46.2 (1992), pp. 381–389. DOI: 10.1111/j.1558-5646.1992.tb02046.x.
- [46] M. C. Whitlock. “Evolutionary inference from Q ST”. In: *Molecular Ecology* 17.8 (2008), pp. 1885–1896. DOI: 10.1111/j.1365-294X.2008.03712.x.

- [47] D. T. Gillespie. “A general method for numerically simulating the stochastic time evolution of coupled chemical reactions”. In: *Journal of Computational Physics* 22.4 (1976), pp. 403–434. DOI: 10.1016/0021-9991(76)90041-3.
- [48] M Kimura and G. H. Weiss. “The stepping stone model of population structure and the decrease of genetic correlation with distance.” In: *Genetics* 49.4 (1964), pp. 561–76. DOI: 10.1093/oxfordjournals.molbev.a025590.
- [49] V. Colizza, R. Pastor-Satorras, and A. Vespignani. “Reactiondiffusion processes and metapopulation models in heterogeneous networks”. In: *Nature Physics* 3.4 (2007), pp. 276–282. DOI: 10.1038/nphys560. arXiv: 0703129 [cond-mat].
- [50] G. Bounova and O. de Weck. “Overview of metrics and their correlation patterns for multiple-metric topology analysis on heterogeneous graph ensembles”. In: *Physical Review E* 85.1 (2012), p. 016117. DOI: 10.1103/PhysRevE.85.016117.
- [51] M. E. J. Newman. “Mixing patterns in networks”. In: *Physical Review E* 67.2 (2003), p. 026126. DOI: 10.1103/PhysRevE.67.026126. arXiv: 0209450 [cond-mat].
- [52] S. Yeaman and S. P. Otto. “Establishment and maintenance of adaptive genetic divergence under migration, selection, and drift”. In: *Evolution* 65.7 (2011), pp. 2123–2129. DOI: 10.1111/j.1558-5646.2011.01277.x.
- [53] B. H. McRae and P. Beier. “Circuit theory predicts gene flow in plant and animal populations”. In: *Proceedings of the National Academy of Sciences* 104.50 (2007), pp. 19885–19890. DOI: 10.1073/pnas.0706568104.
- [54] C. Liu et al. “Mountain metacommunities: climate and spatial connectivity shape ant diversity in a complex landscape”. In: *Ecography* 41.1 (2018), pp. 101–112. DOI: 10.1111/ecog.03067.
- [55] C. Rahbek and G. R. Graves. “Multiscale assessment of patterns of avian species richness”. In: *Proceedings of the National Academy of Sciences of the United States of America* 98.8 (2001), pp. 4534–4539. DOI: 10.1073/pnas.071034898.
- [56] H. Kreft and W. Jetz. “Global patterns and determinants of vascular plant diversity”. In: *Proceedings of the National Academy of Sciences of the United States of America* 104.14 (2007), pp. 5925–5930. DOI: 10.1073/pnas.0608361104.
- [57] R. G. Davies et al. “Topography, energy and the global distribution of bird species richness”. In: *Proceedings of the Royal Society B: Biological Sciences* 274.1614 (2007), pp. 1189–1197. DOI: 10.1098/rspb.2006.0061.

- [58] J. A. Veech and T. O. Crist. “Habitat and climate heterogeneity maintain beta-diversity of birds among landscapes within ecoregions”. In: *Global Ecology and Biogeography* 16.5 (2007), pp. 650–656. DOI: 10.1111/j.1466-8238.2007.00315.x.
- [59] A. Stein, K. Gerstner, and H. Kreft. “Environmental heterogeneity as a universal driver of species richness across taxa, biomes and spatial scales”. In: *Ecology Letters* 17.7 (2014), pp. 866–880. DOI: 10.1111/ele.12277.
- [60] C. Lepers et al. “Inference with selection, varying population size, and evolving population structure: application of ABC to a forwardbackward coalescent process with interactions”. In: *Heredity* 126.2 (2021), pp. 335–350. DOI: 10.1038/s41437-020-00381-x. arXiv: 1910.10201.
- [61] D. Petkova, J. Novembre, and M. Stephens. “Visualizing spatial population structure with estimated effective migration surfaces”. In: *Nature Genetics* 48.1 (2015), pp. 94–100. DOI: 10.1038/ng.3464.
- [62] B. H. McRae. “ISOLATION BY RESISTANCE”. In: *Evolution* 60.8 (2006), p. 1551. DOI: 10.1554/05-321.1.
- [63] F. Altermatt and E. A. Fronhofer. “Dispersal in dendritic networks: Ecological consequences on the spatial distribution of population densities”. In: *Freshwater Biology* 63.1 (2018), pp. 22–32. DOI: 10.1111/fwb.12951.
- [64] J. L. Richardson et al. “Microgeographic adaptation and the spatial scale of evolution”. In: *Trends in Ecology & Evolution* 29.3 (2014), pp. 165–176. DOI: 10.1016/j.tree.2014.01.002.
- [65] M. Slatkin. “GENE FLOW AND SELECTION IN A CLINE”. In: *Genetics* 75.4 (1973), pp. 733–756. DOI: 10.1093/genetics/75.4.733.
- [66] M. Kirkpatrick and N. H. Barton. “Evolution of a Species’ Range”. In: *The American Naturalist* 150.1 (1997), pp. 1–23. DOI: 10.1086/286054.
- [67] J. Polechová and N. H. Barton. “Limits to adaptation along environmental gradients”. In: *Proceedings of the National Academy of Sciences of the United States of America* 112.20 (2015), pp. 6401–6406. DOI: 10.1073/pnas.1421515112.
- [68] M. AndradeRestrepo, N. Champagnat, and R. Ferrière. “Local adaptation, dispersal evolution, and the spatial ecoevolutionary dynamics of invasion”. In: *Ecology Letters* 22.5 (2019). Ed. by V. Calcagno, pp. 767–777. DOI: 10.1111/ele.13234.
- [69] S. Bromberger and other Contributors. “JuliaGraphs/LightGraphs.jl”. In: (2017). DOI: 10.5281/ZENODO.1412141.

- [70] C. Rackauckas and Q. Nie. “DifferentialEquations.jl a performant and feature-rich ecosystem for solving differential equations in Julia”. In: *Journal of Open Research Software* 5 (2017). DOI: 10.5334/jors.151.

2.A Supplementary Note

2.A.1 Mathematical construction of the model

The model is a measure-valued point process [1], so that individuals are represented as dirac functions $\delta_{x_k^{(i)}}$, where $x_k^{(i)} \in \mathcal{X}$ corresponds to the traits' value of individual k located on vertex v_i . Under this formalism, the population on v_i is represented as a sum of dirac functions $\nu_t^{(i)} = \sum_k^{N^{(i)}} \delta_{x_k^{(i)}}$, where $N^{(i)}$ is the local population size. It follows that the time variation of the process can be described by the so-called infinitesimal generator L , defined for all real valued functions ϕ as

$$L\phi(\nu_t^{(i)}) = \partial_t \mathbb{E} [\phi(\nu_t^{(i)})] \quad (\text{S1})$$

(see [2] for an introduction to infinitesimal generators). Equation (S1) provides the expected time variation at time t of e.g. the population size by choosing $\phi(\nu_t^{(i)}) = \int_{\mathcal{X}} \nu_t^{(i)}(dx)$. Recall that we use $b^{(i)}$ to denote the birth rate on vertex v_i , d for the death rate, μ for the mutation probability, m for the migration probability, $\mathcal{M}(x, y) = \frac{1}{\sqrt{2\pi\sigma_\mu}} \exp\left(\frac{\|x-y\|^2}{2\sigma_\mu}\right)$ for the mutation kernel, K for the local carrying capacity, $A = (a_{i,j})_{1 \leq i,j \leq M}$ for the adjacency matrix of the graph G , and $D = (d_1, d_2, \dots, d_M)$ for the vector containing the degree of each vertex. In order to explicitly write the generator L , let us recall that five events of different natures can alter the number of individuals with trait x on vertex v_i :

- an individual on v_i with trait x can give birth to an offspring that does not experience mutations nor migration, at rate $(1 - \mu)(1 - m)b^{(i)}(x)$,
- an individual on v_i with trait y can give birth to an offspring with mutated trait x that does not experience migration, at rate $\mu(1 - m)\mathcal{M}(x, y)b^{(i)}(y)$,
- an individual on v_i with trait x can die, at rate $d(N^{(i)}) = \frac{N^{(i)}}{K} = \frac{1}{K} \int_{\mathcal{X}} \nu_t^{(i)}(dx)$,
- an individual on v_j with trait x can give birth to an offspring that does not experience mutations and migrates to v_i , at rate $\frac{a_{i,j}}{d_j}(1 - \mu)m b^{(j)}(x)$,
- an individual on v_j with trait y can give birth to an offspring with mutated trait x that migrates to v_i , at rate $\frac{a_{i,j}}{d_j}\mu m \mathcal{M}(x, y)b^{(j)}(x)$.

Summing over all all individuals and all vertices yields

$$\begin{aligned}
L\phi(\nu_t^{(i)}) &= \int_{\mathcal{X}} \left\{ b^{(i)}(\mathbf{x})(1-\mu)(1-m)(\phi(\nu_t^{(i)} + \delta_{\mathbf{x}}) - \phi(\nu_t^{(i)})) \right\} \nu_t^{(i)}(d\mathbf{x}) && \text{births w/o mutations, w/o migrations} \\
&+ \int_{\mathcal{X}} \left\{ \mu(1-m) \int_{\mathcal{X}} b^{(i)}(y)(\phi(\nu_t^{(i)} + \delta_z) - \phi(\nu_t^{(i)})) \mathcal{M}(\mathbf{x}, y) dy \right\} \nu_t^{(i)}(d\mathbf{x}) && \text{births w/ mutations, w/o migrations} \\
&+ \iint_{\mathcal{X}} \left\{ \frac{1}{K} (\phi(\nu_t^{(i)} - \delta_{\mathbf{x}}) - \phi(\nu_t^{(i)})) \nu_t^{(i)}(dy) \nu_t^{(i)}(dx) \right\} \\
&+ \sum_{j \neq i} \frac{a_{i,j}}{d_j} \int_{\mathcal{X}} \mu m \left\{ \int_{\mathcal{X}} b^{(j)}(y)(\phi(\nu^{(j)} + \delta_{\mathbf{x}}) - \phi(\nu^{(j)})) \mathcal{M}(\mathbf{x}, y) dy \right\} \nu_t^{(j)}(d\mathbf{x}) && \text{migrations w/o mutations} \\
&+ \sum_{j \neq i} \frac{a_{i,j}}{d_j} \int_{\mathcal{X}} \left\{ b^{(j)}(\mathbf{x})(1-\mu)m(\phi(\nu^{(j)} + \delta_{\mathbf{x}}) - \phi(\nu^{(j)})) \right\} \nu_t^{(j)}(d\mathbf{x}). && \text{migrations w/ mutations}
\end{aligned} \tag{S2}$$

Taking expectations in Eq. (S2), one can obtain an equation for the mean trajectory of the quantity of interest, $\mathbb{E}[\phi(\nu_t^{(i)})]$. Nonetheless, Eq. (S2) involves an integral with respect to $\nu_t^{(i)}(dx)\nu_t^{(i)}(dy)$, making it impossible to obtain an explicit solution. It is therefore unclear whether one can gain insight into the stochastic dynamics from Eq. (S2) without simplifying assumptions. We refer to [3] for a detailed discussion on the topic.

2.A.2 Deterministic approximation

One strategy to overcome the difficulties encountered above is to assimilate the process to its mean trajectory, assuming that $\mathbb{E}[\nu_t^{(i)}] \approx \nu_t^{(i)}$ and further approximating $\nu_t^{(i)}$ with a continuous deterministic function $n_t^{(i)}$. Such strategy inherently neglects the stochasticity of the process, which is reasonable provided that a force dampens the stochastic fluctuations of the quantity of interest.

Setting with no selection

Consider a setting with no selection and recall that in this setting where $x \equiv u \in \mathcal{X} = \mathcal{U}$ we define

$$b^{(i)}(x) \equiv b \tag{S3}$$

By applying the strategy mentioned above and choosing $\phi(n_t^{(i)}) = \int_{\mathcal{X}} n_t^{(i)}(x) dx$, Eq. (S2) transforms into the deterministic approximation of the population size dynamics given in the main-text by

$$\partial_t N_t^{(i)} = N_t^{(i)} \left[b(1-m) - \frac{N_t^{(i)}}{K} \right] + mb \sum_{j \neq i} \frac{a_{i,j}}{d_j} N_t^{(j)}. \quad (\text{S4})$$

Competition stabilises the population size dynamics, which behaves deterministically. This is supported by Fig. S10a, which shows how Eq. (S4) accurately describes the population size for varying migration regimes. Nonetheless, stochastic fluctuations drive the dynamics of the neutral trait distribution. Attempting to characterise the neutral trait distribution with the same strategy, this time setting $\phi(n_t^{(i)}) = n_t^{(i)}(u)$, yields

$$\begin{aligned} \partial_t n_t^{(i)}(u) &= n_t^{(i)}(u) \left[b(1-m)(1-\mu) - \frac{1}{K} \int_{\mathcal{U}} n_t^{(i)}(\mathbf{u}) d\mathbf{u} \right] \\ &\quad + (1-m)\mu b \int_{\mathcal{U}} n_t^{(i)}(\mathbf{u}) \mathcal{M}(u, \mathbf{u}) d\mathbf{u} \\ &\quad + m\mu b \sum_{j \neq i} \frac{a_{i,j}}{d_j} \int_{\mathcal{U}} n_t^{(j)}(u) \mathcal{M}(u, \mathbf{u}) d\mathbf{u} \\ &\quad + m(1-\mu)b \sum_{j \neq i} \frac{a_{i,j}}{d_j} b n_t^{(j)}(u). \end{aligned} \quad (\text{S5})$$

Solving for Eq. (S5), one can show that the variance of $n_t^{(i)}$ continuously grows in time (see Fig. S10) and tends to infinity as time goes to infinity, which is an unrealistic behaviour considering finite populations. Intuitively, this reflects the fact that no stabilising force acts on the neutral trait distribution, such that random fluctuations play a major role in driving the dynamics of the stochastic process. Figure S10 shows how IBM trajectories significantly differ from Eq. (S5), and Fig. S11 illustrates how diversity metrics obtained from Eq. (S5) do not match those obtained from simulations of the IBM.

Setting with heterogeneous selection

In contrast to the neutral trait dynamics, the adaptive distribution can successfully be approximated by a deterministic description because selection pressure acts as a stabilising force and stabilises the populations' adaptive trait, dampening the

stochastic fluctuations. Consider the setting with heterogeneous selection and recall that in this setting where $x \equiv (s, u) \in \mathcal{X} = \mathcal{S} \times \mathcal{U}$ we define

$$b^{(i)}(x) \equiv b(1 - p(s - \theta_i)^2). \quad (\text{S6})$$

By applying the same strategy as above to characterise the adaptive trait distribution $n_t^{(i)}(s)$ by choosing $\phi(n_t^{(i)}) = n_t^{(i)}(s) \equiv \int_{\mathcal{U}} n_t^{(i)}(u, s) du$, Eq. (S2) transforms into

$$\begin{aligned} \partial_t n_t^{(i)}(s) &= n_t^{(i)}(s) \left[b^{(i)}(s)(1-m)(1-\mu) - \frac{1}{K} \int_{\mathcal{S}} n_t^{(i)}(\mathbf{s}) d\mathbf{s} \right] \\ &\quad + (1-m)\mu \int_{\mathcal{S}} b^{(i)}(\mathbf{s}) n_t^{(i)}(\mathbf{s}) \mathcal{M}(\mathbf{s}, s) d\mathbf{s} \\ &\quad + m\mu \sum_{j \neq i} \frac{a_{i,j}}{d_j} \int_{\mathbb{R}} b^{(j)}(\mathbf{s}) n_t^{(j)}(s) \mathcal{M}(\mathbf{s}, s) d\mathbf{s} \\ &\quad + m(1-\mu) \sum_{j \neq i} \frac{a_{i,j}}{d_j} b^{(j)}(s) n_t^{(j)}(s). \end{aligned} \quad (\text{S7})$$

Assuming that the variance of the mutation kernel is small, one can use a diffusion approximation for the mutation term [4, 5, 6]

$$\int_{\mathcal{S}} b^{(i)}(\mathbf{s}) n_t^{(i)}(\mathbf{s}) \mathcal{M}(\mathbf{s}, s) d\mathbf{s} = b^{(i)}(s, t) n_t^{(i)}(s) + \frac{1}{2} \sigma_{\mu}^2 \Delta_s (b^{(i)} n_t^{(i)})(s). \quad (\text{S8})$$

Neglecting the terms in $m\mu$, we obtain

$$\begin{aligned} \partial_t n_t^{(i)}(s) &= n_t^{(i)}(s) \left[b^{(i)}(s, t)(1-m-\mu) - \frac{1}{K} \int_{\mathcal{S}} n_t^{(i)}(\mathbf{s}) d\mathbf{s} \right] \\ &\quad + \mu \left[b^{(i)}(s, t) n_t^{(i)}(s) + \frac{1}{2} \sigma_{\mu}^2 \Delta_s (b^{(i)} n_t^{(i)})(s) \right] \\ &\quad + m \sum_{j \neq i} b^{(j)}(s, t) n_t^{(j)}(s) a_{i,j} \end{aligned} \quad (\text{S9})$$

which, after rearranging terms, yields the elegant deterministic approximation of the adaptive trait dynamics

$$\partial_t n_t^{(i)}(s) = n_t^{(i)}(s) \left[b^{(i)}(s)(1-m) - \frac{1}{K} \int_{\mathcal{S}} n_t^{(i)}(\mathbf{s}) d\mathbf{s} \right] + m \sum_{j \neq i} b^{(j)}(s) \frac{a_{i,j}}{d_j} n_t^{(j)}(s) + \frac{1}{2} \mu \sigma_{\mu}^2 \Delta_s [b^{(i)}(s) n_t^{(i)}(s)]. \quad (\text{S10})$$

Setting $m = 0$ [6] shows that Eq. (S10) admits a stationary solution that is Gaussian, with variance $\sqrt{\mu \sigma_{\mu}^2} / \sqrt{p}$. Therefore, the variance of the adaptive trait distribution stabilises to a finite value. Intuitively, this reflects the fact that the random fluctuations of the adaptive trait distribution are dampened by the stabilising force of selection. Provided that the selection strength p is large enough, Eq. (S10) is a good approximation of the adaptive trait distribution obtained from the stochastic process.

Figure S3 shows how IBM trajectories are similar to the ones obtained from Eq. (S5), and Fig. S4 illustrates how diversity metrics obtained from Eq. (S5) match those obtained from simulations of the IBM.

2.A.3 Trait-dependent competition

To test whether the effects of the metrics hold under more complex ecological processes, we designed an extra experiment considering heterogeneous selection and adaptive trait-dependent competition, where the death rate of individuals on v_i with traits $x_k^{(i)} = (u_k^{(i)}, s_k^{(i)}) \in \mathcal{U} \times \mathcal{S}$ is given by

$$d(x_k^{(i)}, \nu^{(i)}) = \frac{1}{K} \int_{\mathcal{S}} \exp\left(-\frac{(s_k^{(i)} - \mathbf{s})^2}{2\sigma_\alpha^2}\right) \nu^{(i)}(\mathbf{s}) \quad (\text{S11})$$

where σ_α is the competition bandwidth. This competition kernel tends to increase the population size, as it decreases the overall competition. The adaptive dynamics theory predicts that when $m = 0$, competition promotes two distinct types of individuals at either side of the adaptive trait optimum for a competition bandwidth $\sigma_\alpha < 1/\sqrt{2p}$, while a single type is observed when $\sigma_\alpha > 1/\sqrt{2p}$ [7]. We performed simulations in both cases for graphs with $M = 7$ vertices and show results of the multivariate regression analyses in Table S5. The analyses demonstrate that the trends reported in the main manuscript remain unchanged in both cases.

2.A.4 Derivation of the habitat assortativity metric r_Θ in binary environments

We demonstrate here how the habitat assortativity r_Θ relates to the conditional probability of habitats being connected, and we show how r_Θ simplifies under mean field assumption.

Following the original definition of [8], habitat assortativity r_Θ is defined as the Pearson correlation of environmental conditions θ at either ends of the vertices V of graph G , that is

$$r_\Theta = \frac{\text{Cov}(\Theta_\times, \Theta_\wedge)}{\sqrt{\text{Var}(\Theta_\times)\text{Var}(\Theta_\wedge)}} = \frac{\langle \Theta_\times \Theta_\wedge \rangle - \langle \Theta_\times \rangle \langle \Theta_\wedge \rangle}{\sqrt{(\langle \Theta_\times^2 \rangle - \langle \Theta_\times \rangle^2)(\langle \Theta_\wedge^2 \rangle - \langle \Theta_\wedge \rangle^2)}} \quad (\text{S12})$$

where Θ_{\times} and Θ_{\wedge} denote the sets of environmental conditions found at the toe and tip of each directed vertex of graph V , and $\langle \Theta_{\times} \rangle$ and $\langle \Theta_{\wedge} \rangle$ denote their respective mean values.

Let $P(\bullet, \bullet)$ be the proportion of edges that connect a vertex of habitat type \bullet to a vertex of habitat type \bullet . One can also view $P(\bullet, \bullet)$ as the conditional probability that a vertex of type \bullet is connected to a vertex of type \bullet . Let $P(\bullet)$ denote the proportion of vertices that are of type \bullet . First observe that for undirected graphs, one has $\langle \Theta_{\times} \rangle = \langle \Theta_{\wedge} \rangle$ and $\langle \Theta_{\times}^2 \rangle = \langle \Theta_{\wedge}^2 \rangle$. Assuming that habitats are symmetric and binary, it follows that $\theta_{\bullet} = -\theta_{\bullet}$. Then

$$\begin{aligned}\langle \Theta_{\times} \Theta_{\wedge} \rangle &= P(\bullet, \bullet) \theta_{\bullet}^2 + P(\bullet, \bullet) \theta_{\bullet}^2 + [P(\bullet, \bullet) + P(\bullet, \bullet)] \theta_{\bullet} \theta_{\bullet} \\ &= \theta_{\bullet}^2 (P(\bullet, \bullet) + P(\bullet, \bullet)) - [P(\bullet, \bullet) + P(\bullet, \bullet)],\end{aligned}\quad (\text{S13})$$

$$\begin{aligned}\langle \Theta_{\times} \rangle &= P(\bullet) \theta_{\bullet} + P(\bullet) \theta_{\bullet} \\ &= \theta_{\bullet} [P(\bullet) - P(\bullet)],\end{aligned}\quad (\text{S14})$$

$$\begin{aligned}\langle \Theta_{\times}^2 \rangle &= P(\bullet) \theta_{\bullet}^2 + P(\bullet) \theta_{\bullet}^2 \\ &= \theta_{\bullet}^2 [P(\bullet) + P(\bullet)] \\ &= \theta_{\bullet}^2.\end{aligned}\quad (\text{S15})$$

Combining Eq. (S13), Eq. (S14) and Eq. (S15) with Eq. (S12) one gets

$$\begin{aligned}r_{\Theta} &= \frac{\langle \Theta_{\times} \Theta_{\wedge} \rangle - \langle \Theta_{\times} \rangle \langle \Theta_{\wedge} \rangle}{\langle \Theta_{\times}^2 \rangle - \langle \Theta_{\times} \rangle^2} \\ &= \frac{P(\bullet, \bullet) + P(\bullet, \bullet) - [P(\bullet, \bullet) + P(\bullet, \bullet)] - (P(\bullet) - P(\bullet))^2}{P(\bullet) + P(\bullet) - (P(\bullet) - P(\bullet))^2} \\ &= \frac{P(\bullet, \bullet) + P(\bullet, \bullet) - [P(\bullet, \bullet) + P(\bullet, \bullet)] - (P(\bullet) - P(\bullet))^2}{1 - (P(\bullet) - P(\bullet))^2}.\end{aligned}\quad (\text{S16})$$

Assuming that habitats are homogeneously distributed, we have $P(\bullet) = P(\bullet) = \frac{1}{2}$ and thus we obtain

$$r_{\Theta} = P(\bullet, \bullet) + P(\bullet, \bullet) - [P(\bullet, \bullet) + P(\bullet, \bullet)].\quad (\text{S17})$$

The mean field approximation involves the assumption that all vertices with similar habitats are equivalent in terms of their connections with other habitats, so that $P(\bullet, \bullet) = P(\bullet, \bullet)$ and $P(\bullet, \bullet) = P(\bullet, \bullet)$, which yields $r_{\Theta} = 2(P(\bullet, \bullet) - P(\bullet, \bullet))$.

References

- [1] V. Bansaye and S. Méléard. “Some stochastic models for structured populations : scaling limits and long time behavior”. In: *Stochastic Models for Structured Populations: Scaling Limits and Long Time Behavior* (2015), pp. 1–107. DOI: 10.1007/978-3-319-21711-6. arXiv: 1506.04165.
- [2] H. Linke. “Applications of Brownian Motion”. In: 5114 (2015), pp. 199–213. DOI: 10.1142/9789814678940_0009.
- [3] N. Champagnat, R. Ferrière, and S. Méléard. “Unifying evolutionary dynamics: From individual stochastic processes to macroscopic models”. In: *Theoretical Population Biology* 69.3 (2006), pp. 297–321. DOI: 10.1016/j.tpb.2005.10.004.
- [4] M. Kimura. “A stochastic model concerning the maintenance of genetic variability in quantitative characters.” In: *Proceedings of the National Academy of Sciences of the United States of America* 54.3 (1965), pp. 731–736. DOI: 10.1073/pnas.54.3.731.
- [5] F. Débarre, O. Ronce, and S. Gandon. “Quantifying the effects of migration and mutation on adaptation and demography in spatially heterogeneous environments”. In: *Journal of Evolutionary Biology* 26.6 (2013), pp. 1185–1202. DOI: 10.1111/jeb.12132.
- [6] S. Mirrahimi and S. Gandon. “Evolution of specialization in heterogeneous environments: equilibrium between selection, mutation and migration”. In: *Genetics* 214.2 (2020), pp. 479–491. DOI: 10.1534/genetics.119.302868.
- [7] M. Doebeli. *Adaptive diversification*. Monographs in population biology. Princeton, N.J: Princeton University Press, 2011.
- [8] M. E. J. Newman. “Mixing patterns in networks”. In: *Physical Review E* 67.2 (2003), p. 026126. DOI: 10.1103/PhysRevE.67.026126. arXiv: 0209450 [cond-mat].
- [9] W.-N. Ding et al. “Ancient orogenic and monsoon-driven assembly of the world’s richest temperate alpine flora”. In: *Science* 369.6503 (2020), pp. 578–581. DOI: 10.1126/science.abb4484.
- [10] M. Jung et al. “A global map of terrestrial habitat types”. In: *Scientific Data* 7.1 (2020), p. 256. DOI: 10.1038/s41597-020-00599-8.
- [11] D. N. Karger et al. “Climatologies at high resolution for the earth’s land surface areas”. In: *Scientific Data* 4.1 (2017), p. 170122. DOI: 10.1038/sdata.2017.122. arXiv: 1607.00217.

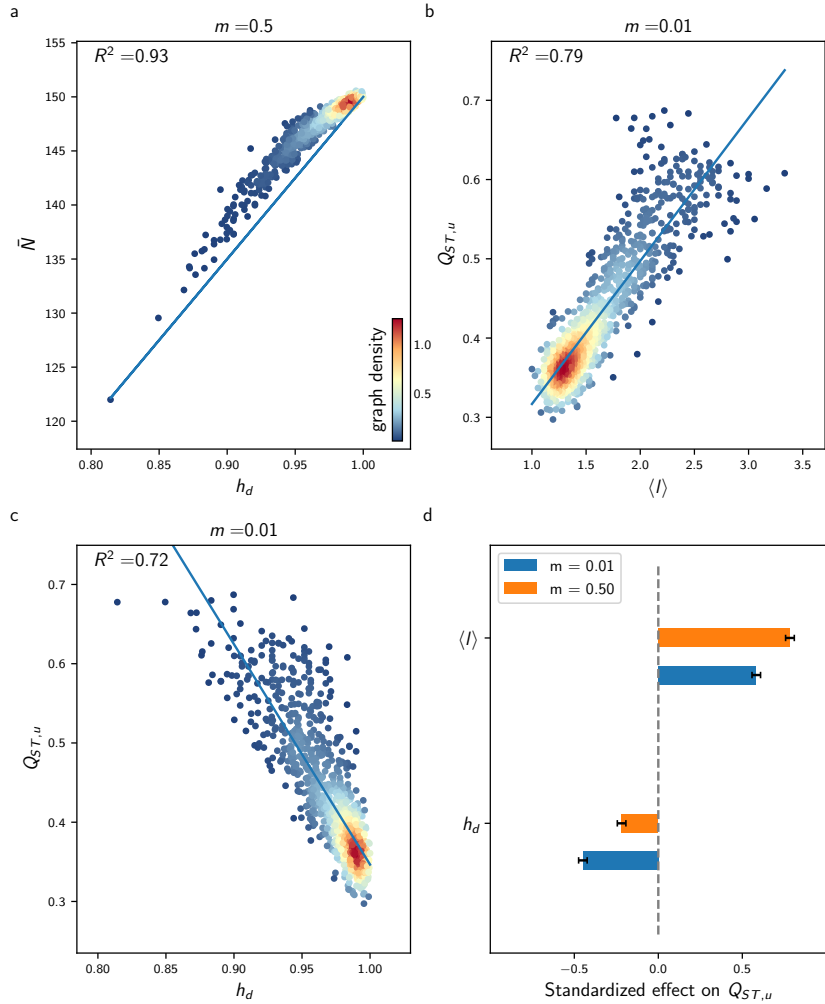


Fig. S1: Effect of $\langle l \rangle$ and h_d on average population size \bar{N} and neutral differentiation $Q_{ST,u}$ under the setting with no selection, analogous to Fig. 2.2 but for 1126 of the 261,080 undirected connected graphs with $M = 9$ vertices.

2.B Supplementary Figures

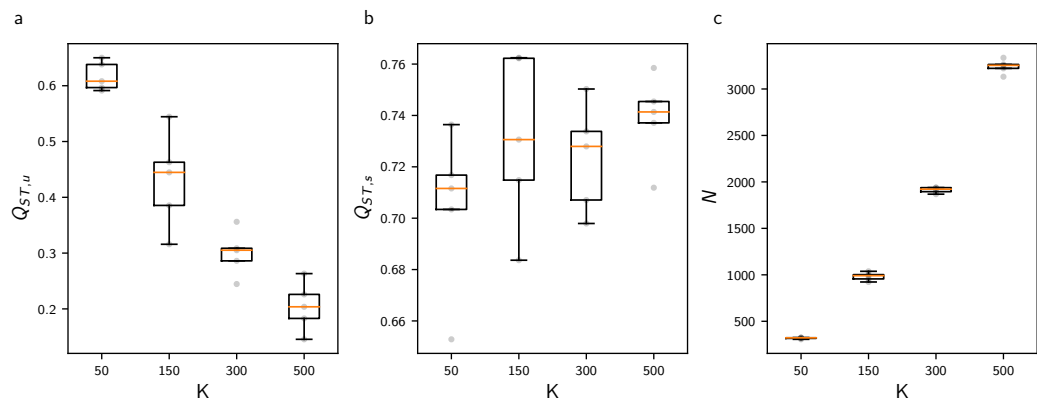


Fig. S2: Effect of the carrying capacity K on $Q_{ST,u}$, $Q_{ST,s}$ and metapopulation size N for the line graph with $M = 7$ vertices for $m = 0.1$. Decreasing K increases $Q_{ST,u}$ as it favours drift, but it does not influence $Q_{ST,s}$. Each boxplot is based on 5 replicate simulations of the IBM, and fade dots represent single values for each replicate.

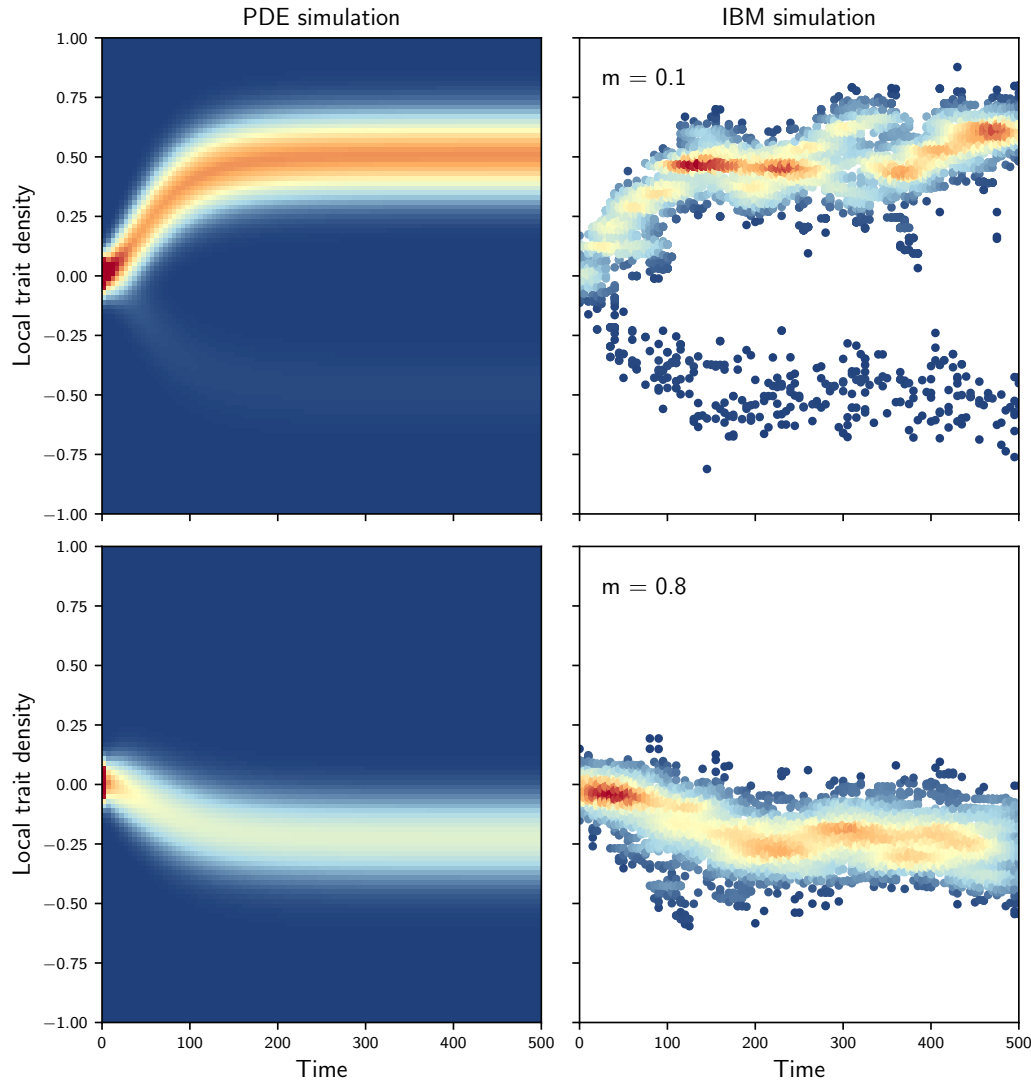


Fig. S3: Comparison of the adaptive trait density on one vertex obtained from Eq. (S10) (left) and from the IBM simulations (right) in the setting with heterogeneous selection, for the star graph with $M = 7$ vertices. The densities obtained from Eq. (S10) and from the IBM are qualitatively similar.

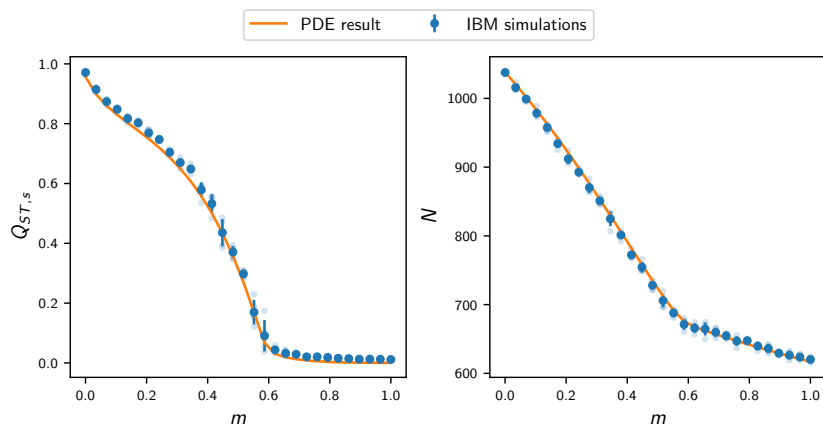


Fig. S4: Comparison of $Q_{ST,s}$ and N obtained from the deterministic approximation Eq. (S10) and from IBM simulations in the setting with heterogeneous selection, on the star graph with $M = 7$ vertices. $Q_{ST,s}$ and population size obtained from Eq. (S10) closely match the IBM simulations. Each plain dot represents average results from 5 replicate simulations of the IBM, bars represent one standard deviation, and each fade dot represents a single replicate value.

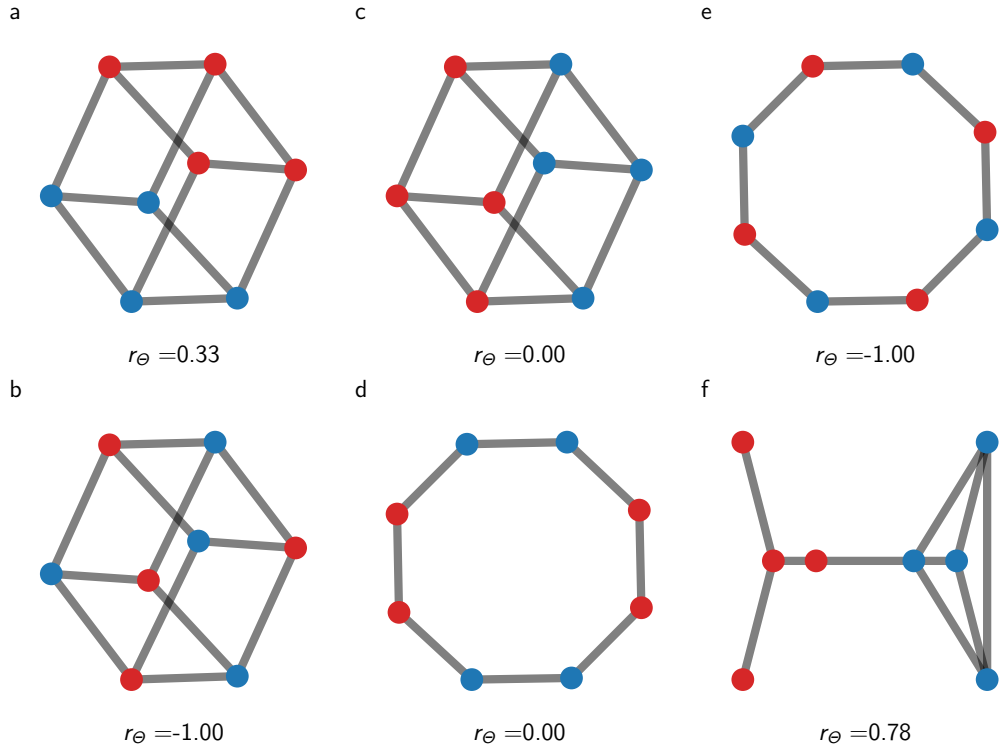


Fig. S5: Graphs with spatial distribution of habitat types corresponding to different habitat assortativity r_Θ . Graphs (ad) can be described exactly with a mean field approach, as blue and red vertices have an equivalent position on the graph.

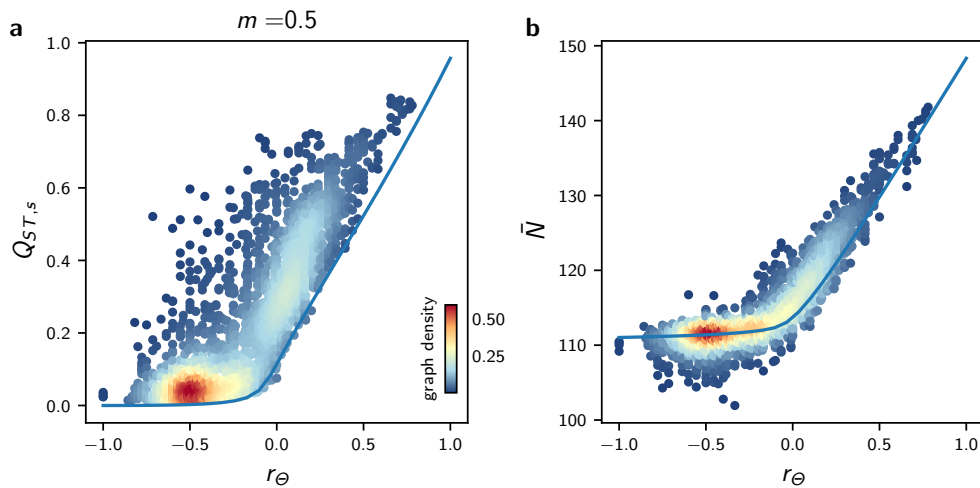


Fig. S6: Effects of habitat heterogeneity r_Θ on $Q_{ST,s}$ and average population size \bar{N} for all undirected connected graphs with $M = 7$ vertices and varying r_Θ , obtained for similar simulations to those in Fig. 2.4 with $m = 0.5$. In (a) and (b), each dot represents average results from 5 replicate simulations of the IBM, the colour scale corresponds to the proportion of the graph with similar x and y axis values (graph density), and the blue lines correspond to results obtained from the mean field, deterministic approximation Eq. (2.5). Deviations from the mean field, deterministic approximation Eq. (2.5) can be explained by differences in $\langle l \rangle$ and h_d between the graphs.

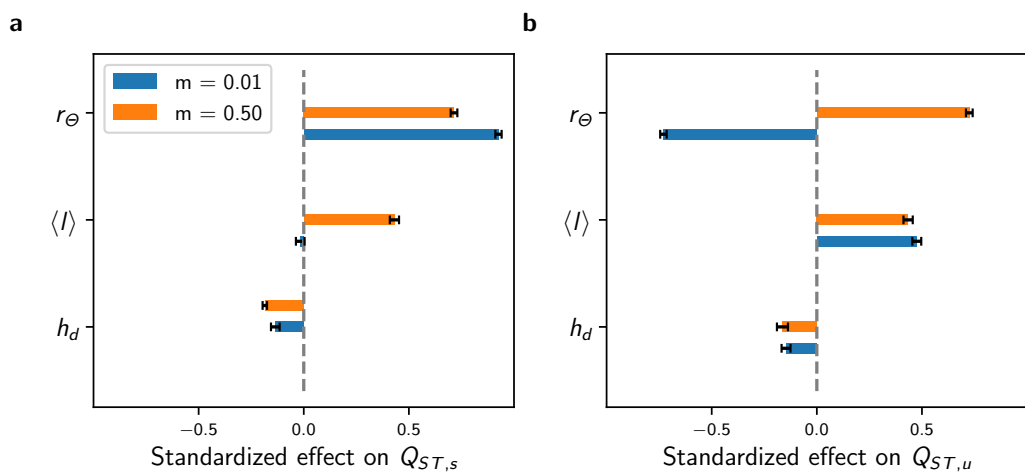


Fig. S7: Standardized effects of h_d , $\langle l \rangle$ and r_Θ on $Q_{ST,s}$ and $Q_{ST,u}$ obtained from multivariate regression models independently fitted for low and high migration regimes on average results from 5 replicate simulations of the IBM, analogous Fig. 2.5c-d but for 1126 of the 261,080 undirected connected graphs with $M = 9$ vertices and varying r_Θ (see Methods for details). Error bars show 95% confidence intervals.

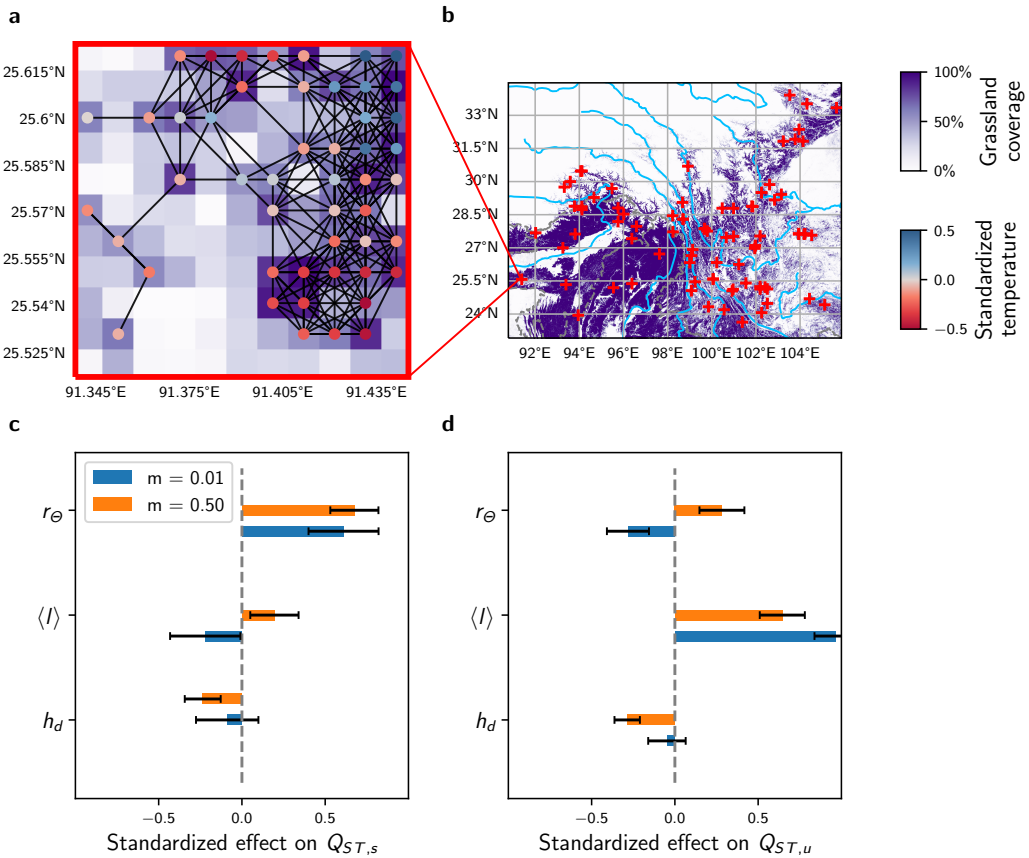


Fig. S8: Simulations on graphs with $M = 49$ vertices obtained from real spatial habitat datasets, in the setting with heterogeneous selection. The region from where graphs are obtained is centred on the Hengduan Mountains in Southwest China, one of the most species-rich temperate mountain biota globally [9]. (a) Graphical representation of a geographical area of size $0.11^\circ \times 0.11^\circ$. To create the graph, we considered biological populations living in grasslands, and used the dataset provided in [10] containing global grassland coverage at 0.01° resolution. We assigned a vertex to a geographical area of size $0.01^\circ \times 0.01^\circ$ if its grassland coverage was above a threshold arbitrarily set to 50%. We further assumed that two vertices were connected if their euclidean distance was below a certain dispersal range, which we let vary from 1 to 2.5 km. Local annual average temperature was considered as the value that captures environmental conditions at each vertex. Temperature data was obtained from the CHELSA dataset [11]. (b) Grassland coverage for the considered region. Blue lines correspond to rivers and dashed grey lines correspond to country borders. Red crosses indicate the locations of the 83 graphs sampled for the simulations used in (c-d). (c-d) Standardized effects of h_d , $\langle l \rangle$ and r_Θ on $Q_{ST,s}$ and $Q_{ST,u}$ obtained from multivariate regression models independently fitted for low and high migration regimes to average results from 5 replicate simulations of the IBM on the 83 graphs which location is illustrated in (c) (see Table S4 for simulation details). Error bars show 95% confidence intervals.

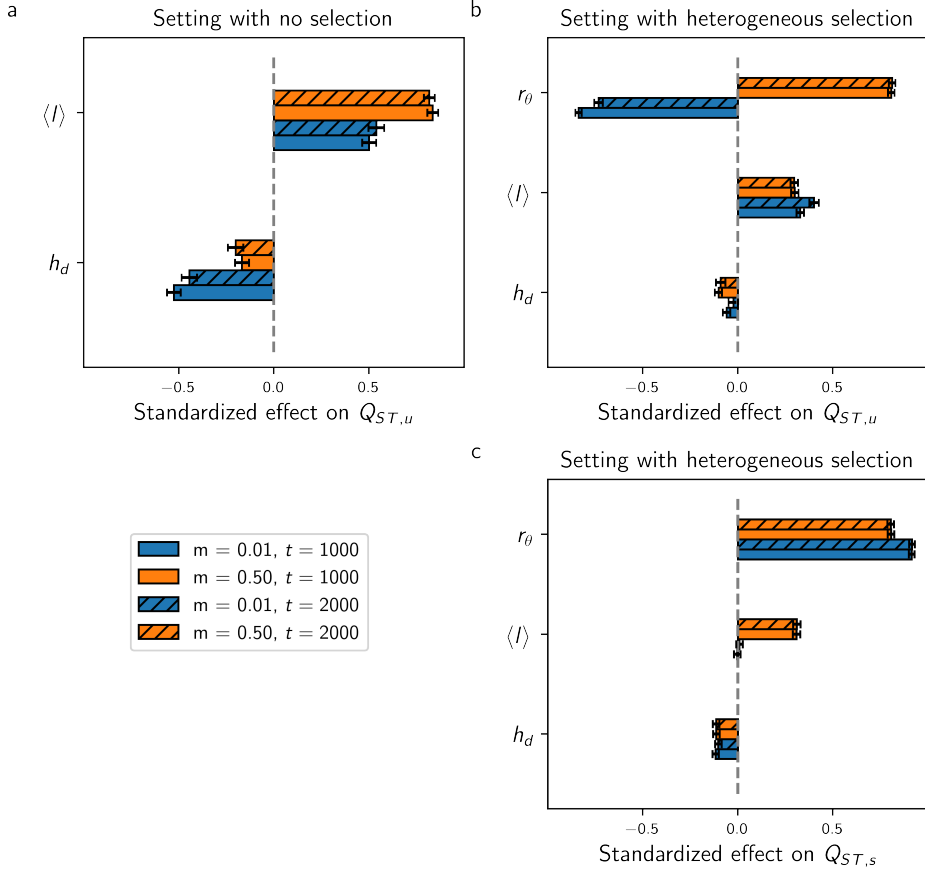


Fig. S9: Standardized effects of h_d , $\langle l \rangle$ and r_Θ on $Q_{ST,u}$ in the setting with no selection and in the setting with heterogeneous selection for the time horizons $t = 1000$ and $t = 2000$, obtained from multivariate regression models independently fitted for low and high migration regimes to average results from 5 replicate simulations of the IBM on all undirected connected graphs with $M = 7$ vertices and varying r_Θ (see Methods for details). (a–c) illustrate that the effects of the topology metrics on $Q_{ST,u}$ and $Q_{ST,s}$ remain constant for $t > 1000$ in both the settings without selection and with heterogeneous selection. Error bars show 95% confidence intervals.

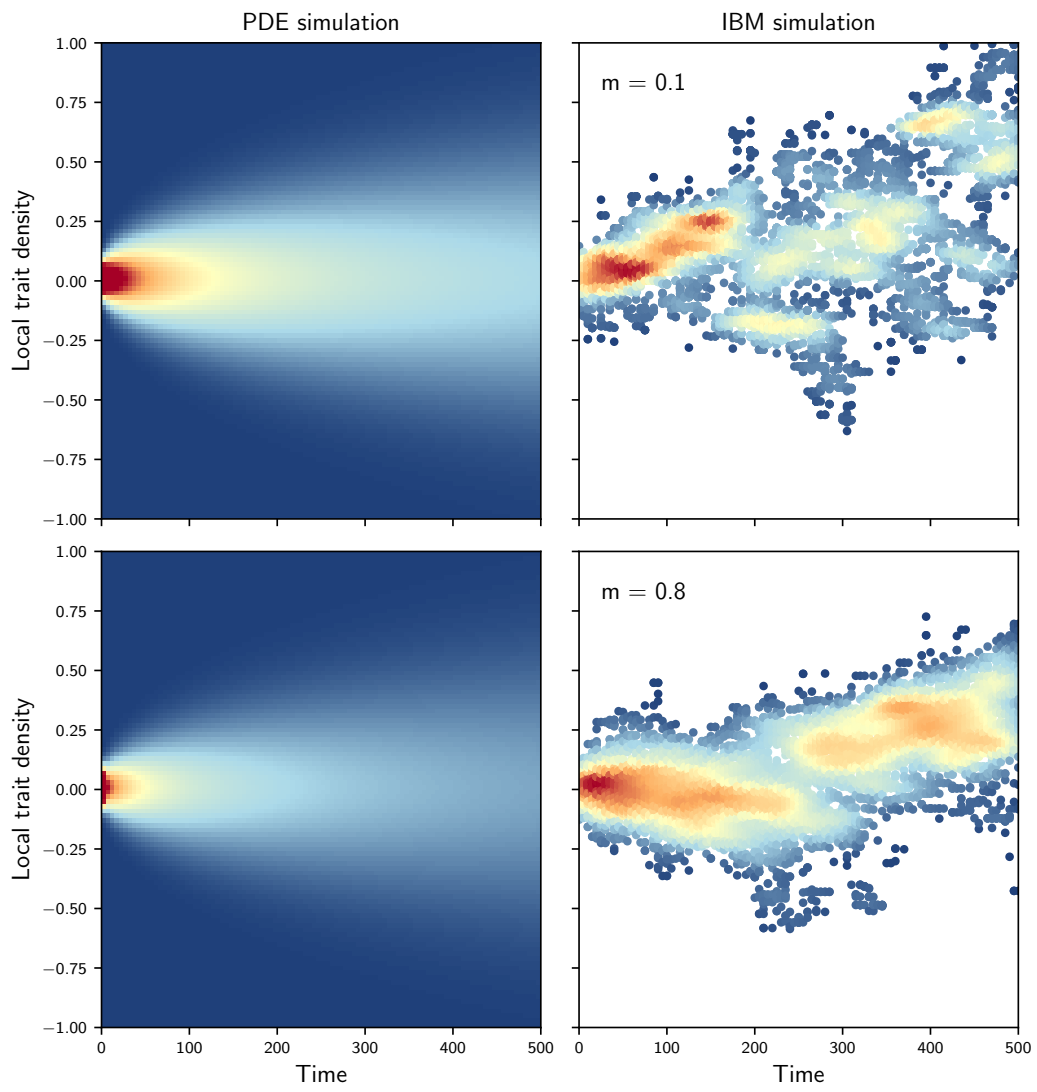


Fig. S10: Comparison of the neutral trait density on one vertex obtained from Eq. (S5) (left) and from the IBM simulations (right) in the setting with no selection, for the chain graph. The densities obtained from Eq. (S5) and from the IBM are dissimilar.

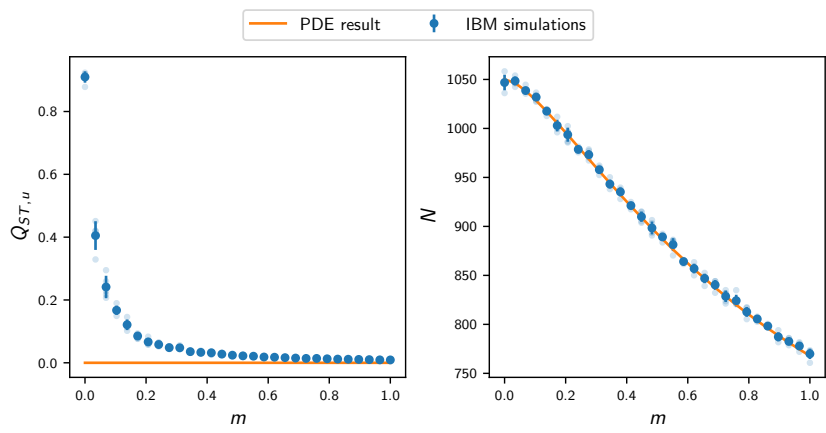


Fig. S11: Comparison of results obtained from the deterministic approximations Eqs. (S4) and (S5) and from IBM simulations in the setting with no selection, on the star graph with $M = 7$ vertices. While Eq. (S4) can capture population size, Eq. (S5) is not able to capture $Q_{ST,u}$. Each plain dot represents average results from 5 replicate simulations, bars represent one standard deviation, and each fade dot represents a single replicate value.

2.C Supplementary Tables

Tab. S1: Linear regression model coefficients for the effect of topology metrics on $Q_{ST,u}$ in the setting with no selection, based on all graphs with $M = 7$ vertices. *** $P < 0.001$

m	$Q_{ST,u}$				$Q_{ST,u} - bN$	
	0.01	0.50	0.01	0.50	0.01	0.50
(Intercept)	0.000 (0.023)	-0.000 (0.017)	-0.000 (0.023)	-0.000 (0.025)	-0.000 (0.023)	-0.000 (0.028)
$\langle l \rangle$	0.739*** (0.023)	0.872*** (0.017)				
h_d			-0.753*** (0.023)	-0.674*** (0.025)	-0.753*** (0.023)	-0.143*** (0.028)
Number of sim.	853	853	853	853	853	853
R^2	0.546	0.760	0.567	0.454	0.567	0.030

Tab. S2: Multivariate linear regression model coefficients for the effect of topology metrics on $Q_{ST,u}$ in the setting with no selection. *** $P < 0.001$

m	$M = 7$				$M = 9$	
	$Q_{ST,u}$					
	0.01	0.50	0.01	0.50		
(Intercept)	-0.000 (0.017)	-0.000 (0.013)	0.000 (0.009)	-0.000 (0.010)		
h_d	-0.527*** (0.019)	-0.352*** (0.014)	-0.449*** (0.013)	-0.218*** (0.013)		
$\langle l \rangle$	0.500*** (0.019)	0.712*** (0.014)	0.583*** (0.013)	0.784*** (0.013)		
Number of sim.	853	853	1,126	1,126		
R^2	0.766	0.858	0.899	0.896		

Tab. S3: Multivariate linear regression model coefficients for the effect of the topology metrics on $Q_{ST,u}$ and $Q_{ST,s}$ in the setting with heterogeneous selection. *** $P < 0.001$

m	$M = 7$				$M = 9$			
	$Q_{ST,s}$		$Q_{ST,u}$		$Q_{ST,s}$		$Q_{ST,u}$	
	0.01	0.50	0.01	0.50	0.01	0.50	0.01	0.50
(Intercept)	-0.000 (0.008)	-0.000 (0.009)	-0.000 (0.009)	-0.000 (0.009)	0.000 (0.008)	0.000 (0.008)	0.000 (0.008)	0.000 (0.008)
h_d	-0.117*** (0.009)	-0.114*** (0.010)	-0.060*** (0.010)	-0.102*** (0.010)	-0.135*** (0.010)	-0.185*** (0.011)	-0.146*** (0.011)	-0.164*** (0.011)
$\langle l \rangle$	-0.004 (0.009)	0.309*** (0.010)	0.328*** (0.010)	0.300*** (0.010)	-0.017 (0.010)	0.431*** (0.011)	0.475*** (0.011)	0.434*** (0.011)
r_Θ	0.914*** (0.008)	0.805*** (0.009)	-0.838*** (0.009)	0.807*** (0.009)	0.926*** (0.008)	0.715*** (0.008)	-0.730*** (0.008)	0.725*** (0.008)
Number of sim.	2,548	2,548	2,548	2,548	2,250	2,250	2,250	2,250
R^2	0.845	0.808	0.808	0.799	0.870	0.853	0.862	0.851

Tab. S4: Multivariate linear regression model coefficients for the effect of topology metrics on $Q_{ST,u}$ and $Q_{ST,s}$ on real graphs with $M = 49$ vertices in the setting with heterogeneous selection. * $P < 0.05$, ** $P < 0.01$, *** $P < 0.001$

m	$Q_{ST,s}$		$Q_{ST,u}$	
	0.1	0.50	0.1	0.50
(Intercept)	-0.000 (0.093)	-0.000 (0.064)	0.000 (0.056)	-0.000 (0.059)
h_d	-0.088 (0.094)	-0.235*** (0.065)	-0.048 (0.057)	-0.286*** (0.060)
$\langle l \rangle$	-0.220* (0.106)	0.195** (0.073)	0.965*** (0.064)	0.645*** (0.068)
r_Θ	0.610*** (0.106)	0.675*** (0.073)	-0.282*** (0.063)	0.282*** (0.068)
Number of sim.	83	83	83	83
R^2	0.313	0.675	0.752	0.717

Tab. S5: Multivariate linear regression model coefficients for the effect of topology metrics on $Q_{ST,u}$ and $Q_{ST,s}$ in the setting of trait-dependent competition and heterogeneous selection (Section 2.A.3), based on all graphs with $M = 7$ vertices. *** $P < 0.001$

m	$\sigma_a = 0.5 < 1/\sqrt{2p}$				$\sigma_a = 1 > 1/\sqrt{2p}$			
	$Q_{ST,s}$		$Q_{ST,u}$		$Q_{ST,s}$		$Q_{ST,u}$	
	0.05	0.50	0.05	0.50	0.05	0.50	0.05	0.50
(Intercept)	0.000 (0.005)	-0.000 (0.010)	-0.000 (0.011)	-0.000 (0.010)	0.000 (0.004)	-0.000 (0.008)	0.000 (0.012)	-0.000 (0.007)
h_d	-0.228*** (0.006)	-0.118*** (0.011)	-0.171*** (0.012)	-0.169*** (0.012)	-0.166*** (0.004)	-0.128*** (0.009)	-0.178*** (0.013)	-0.139*** (0.008)
$\langle l \rangle$	0.084*** (0.006)	0.373*** (0.011)	0.461*** (0.012)	0.573*** (0.012)	0.002 (0.004)	0.296*** (0.009)	0.483*** (0.013)	0.286*** (0.008)
r_Θ	0.922*** (0.005)	0.741*** (0.010)	-0.657*** (0.011)	0.508*** (0.010)	0.967*** (0.004)	0.816*** (0.008)	-0.585*** (0.012)	0.837*** (0.007)
Number of sim.	2,548	2,548	2,548	2,548	2,548	2,548	2,548	2,548
R^2	0.934	0.768	0.716	0.732	0.962	0.828	0.659	0.861

3

Curriculum vitae

Personal Information

Personal skills

Education

10.2022	Ph.D in Environmental Sciences, Swiss Federal Institute for Forest, Snow and Landscape (WSL Swiss Federal Institute of Technology Zurich, ETH), Switzerland
09.2018	"Forward and inverse modelling of eco-evolutionary processes". Under the guidance of Prof. Dr. Loïc Pellissier.
06.2017	Full year academic exchange, University of New South Wales (UNSW Sydney), Australia
09.2016	
06.2017	Master thesis in theoretical geomechanics, UNSW Sydney CSIRO, Australia
02.2017	"Numerical continuation and bifurcation analysis for unconventional geomechanics". Under the guidance of Dr. Thomas Poulet.

08.2018	B.S./ M.S. in Energy and Environmental Engineering, Institut National Des Sciences Appliquées de Lyon (INSA Lyon), France
09.2013	<ul style="list-style-type: none"> • Two-year undergraduate intensive course in mathematics and physics. Ranking : 21/650 students. • Three-year undergraduate engineering course in Energy and Environmental Systems, focused on Advanced Energy Systems and Efficiency.

Professional appointments

08.2018	R&D intern, Compagnie National du Rhône (CNR), France
03.2018	<p>Development of an Energy Management System based on various optimisation techniques for optimal production of renewable resources. Applications to EU sponsored projects:</p> <ul style="list-style-type: none"> • Jupiter1000 (power-to-gas) • Move in pure (vehicle-to-grid) • Marie-Galante island (micro-grid)

Publications

Talks

Softwares

MiniBatchInference.jl	2022
github.com/vboussange/MiniBatchInference.jl	
A Julia package for maximum likelihood estimation and model selection of strongly nonlinear dynamical models.	
HighDimPDE.jl	2021
github.com/vboussange/HighDimPDE.jl	
A Julia package that breaks down the curse of dimensionality in solving non local, non linear PDEs.	
EvoId.jl	2019 - 2021
github.com/vboussange/EvoId.jl	
Evolutionary individual based modelling, mathematically grounded.	
OptiVPP	2018
confidential	
Energy Management System for Virtual Power Plants.	
Open Source contributions	
SciML, DiffEqFlux.jl, CUDA.jl, Flux.jl, LightGraphs.jl.	

Teaching and supervision

Reviews

Colophon

This thesis was typeset with L^AT_EX 2_<. It uses the *Clean Thesis* style developed by Ricardo Langner. The design of the *Clean Thesis* style is inspired by user guide documents from Apple Inc.

Download the *Clean Thesis* style at <http://cleanthesis.der-ric.de/>.

